Pergamon

Journal of Structural Geology, Vol. 20, No. 9/10, pp. 1169 to 1189, 1998

0191-8141/98/$ - see front matter

PII: S0191-8141(98)00061-3

Folding and granite emplacement inferred from structural, strain, TEM and gravimetric analyses: the case study of the Tulle antiform, SW French Massif Central

JEAN-YVES ROIG* and MICHEL FAURE†

CNRS UMR 6530, Dépt des Sciences de la Terre, Université d'Orléans, 45060 Orléans Cédex 2, France
E-mail: roig@dr.brgm.fr

and

CATHERINE TRUFFERT

BRGM, SGN, I2G, 45060 Orléans Cédex 2, France

(*Received* 14 *July* 1997; *accepted in revised form* 20 *April* 1998)

Abstract—In the South Limousin (French Massif Central), the Tulle anticline is a kilometre-scale, upright, open fold which re-folds an already foliated Variscan stack of nappes. Three main granodioritic plutons associated with numerous folded dykes and boudinaged sills crop out in the core of the Tulle anticline. Microstructural study, including quartz ⟨*c*⟩-axis petrofabrics and transmission electron microscope (TEM) analysis allows us to recognize the timing of deformation during pluton emplacement and cooling. The earliest fabric is a pre-full crystallization deformation. The second stage corresponds to a high-temperature (*ca* 650°C) solid-state deformation. The last deformation is responsible for the ⟨*c*⟩-axis preferred orientation at low temperature. Several methods of strain analysis applied in various mineral phases show that pluton emplacement is coeval to a constrictional strain. This strain is characterized by a NW–SE maximum stretching axis (*X*) parallel to the Tulle anticline axis and an intermediate, NE–SW-trending, shortening axis (*Y*) also responsible for large open folding of the host rocks. Gravimetric modelling allows us to determine a laccolithic shape for the plutons. Hot Stokes diapirism is ruled out and the hypothesis of granitic magma channelling through dykes is preferred. A laccolith emplacement model based on a syn-folding décollement level is proposed.

INTRODUCTION

The importance of granites as crustal-scale deformation markers is well established (e.g. Gapais, 1987; Hutton, 1988). Structural and textural patterns of granitic bodies strongly depend on their emplacement dynamics and regional tectonics (Castro, 1987). There are often spatial and temporal relationships between regional structures and magmatism. The coincidence of granitic plutonism and major transcurrent shear zones has been recognized for a long time (e.g. Hutton and Reavy, 1992). Granitic bodies are also often found in the core of upright antiforms, domes or metamorphic core complexes (e.g. Soula, 1982; Hill *et al.*, 1992; Holm *et al.*, 1992; Faure *et al.*, 1996). Therefore, structural study of both granitic bodies and host rocks is necessary to understand regional tectonism and pluton emplacement. Moreover, the characterization of the pluton structure is very useful in determining the timing of the regional deformations (Paterson and Tobisch, 1988).

This study deals with structural analysis, kinematics, strain measurements, quartz ⟨*c*⟩-axis orientation and transmission electron microscope (TEM) observations of the ductile structures in granitoids and related dykes that crop out in the core of the Tulle antiform in the Limousin area, French Massif Central. The gravimetric modelling allows us to constrain the three-dimensional shape of the plutons. The relationships between granite emplacement and upright folding are discussed, and a model for granite emplacement coeval with folding is proposed.

GEOLOGICAL SETTING

The lithotectonic units

The French Massif Central (Fig. 1) belongs to the Western Europe Variscan belt which resulted from Silurian–Carboniferous convergence and collision between Gondwana and Baltica (e.g. Matte, 1986). The Variscan geodynamic evolution of the French Massif Central was accompanied by widespread magmatic activity. Four lithotectonic units are recognized (Fig. 1), based on lithologies, ages and structural and metamorphic characteristics (Floc'h, 1983; Ledru and

*Author to whom correspondence should be addressed at (present address): BRGM, DR/MGG, BP 6009 45060 Orléans Cédex 2. France.

†Also at: Institut Universitaire de France at Université d'Orléans, 45060 Orléans Cédex 2, France

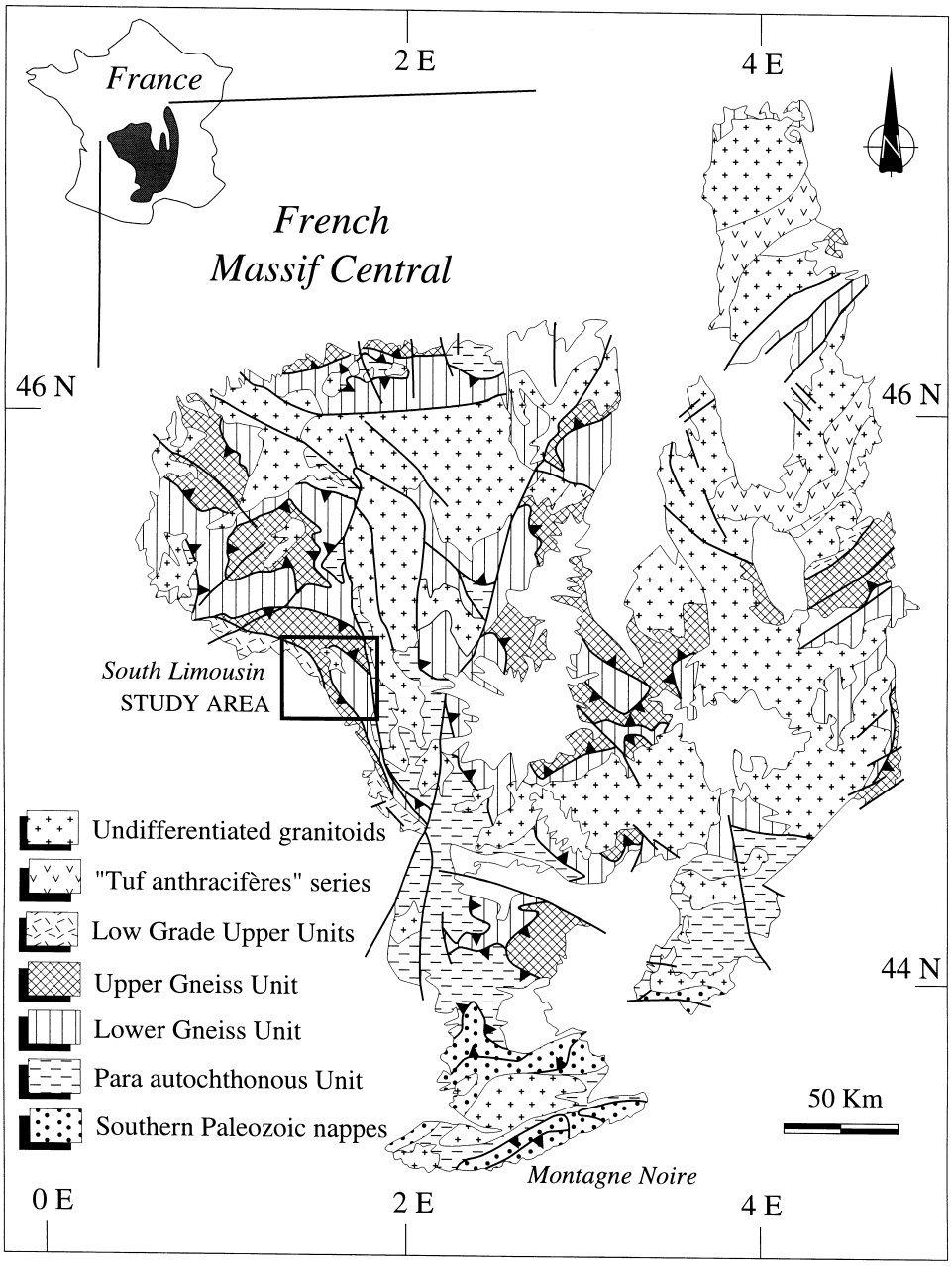

Fig. 1. Structural map of the French Massif Central.

Autran, 1987; Ledru *et al.*, 1989). From top to bottom they are: (i) the low grade Upper Unit, (ii) the Upper Gneiss Unit, (iii) the Lower Gneiss Unit; and (iv) the Para-autochthonous Unit. These four units form the internal zone of the French Massif Central. The southern nappes and recumbent folds in the Montagne Noire are interpreted as the external zone of the belt. The high-pressure metamorphism (eo-Variscan event), dated between 440 and 400 Ma, and recorded in eclogites and high-pressure granulites of the Upper Gneiss Unit is related to a subduction event (Pin and Peucat, 1986). During their exhumation, the high-pressure rocks experienced retrogression to amphibolite facies and partial melting around 390–380 Ma (Duthou, 1977; Lafon, 1986).

The main tectonic event corresponding to the 'Hercynian orogeny proper' occurred around 360 Ma (late Devonian–early Carboniferous) under medium temperature–medium pressure (Barrovian) conditions. A flat-lying foliation and a NW–SE-trending stretching lineation with top-to-the-northwest sense of shear related to this event are widespread in the whole Massif Central (e.g. Floc'h, 1983; Ledru *et al.*, 1989). In early Carboniferous times (*ca* 350 Ma) nappe tectonics were followed by wrenching, upright folding and plutonism. The massifs described below belong to this event.

Lastly, late orogenic extensional tectonics characterized by ductile normal faults, a NW–SE stretching direction and syn-kinematic leucogranite emplacement occurred diachronously throughout Massif Central

(Faure, 1995). In the internal zone, crustal thinning began as soon as late early Carboniferous as shown by the tectonics of the Late Visean 'Tufs anthracifères' series (Fig. 1), while nappe tectonics continued in the external zone. By middle Carboniferous time extensional structures were widespread.

THE SOUTH LIMOUSIN STRUCTURAL PATTERN

The South Limousin area is a relatively small domain where the four structural units of the internal zone are intruded by several granitic bodies (Fig. 2). The low grade Upper Unit, called the Thiviers–Payzac Unit, outcrops in the western part of the study area. It consists of rhyodacitic tuffs and meta-ignimbrites of Cambrian age, and Ordovician–Silurian marine sediments (Guillot, 1981). In this unit the metamorphism corresponds to greenschist- to lower amphibolite-facies conditions. The exact geometry of the Thiviers–Payzac Unit with respect to the high-grade rocks of the Upper Gneiss Unit is still debated. The Tournaisian left-lateral Estivaux transcurrent shear zone at the contact between the Thiviers–Payzac Unit and the Upper Gneiss Unit has obliterated the primary relationships. The Estivaux granodiorite which outcrops along the fault zone has been demonstrated to be a syn-kinematic pluton emplaced during the left-lateral shearing (Roig *et al.*, 1996). The Upper Gneiss Unit is composed of paragneiss with several lenses of mafic and ultramafic rocks. Some of them record an eclogitic metamorphism related to the late Silurian subduction event (Santallier, 1981; Pin and Peucat, 1986). Most of the metamorphic assemblages correspond to the amphibolite facies attributed to the early Carboniferous (*ca* 360 Ma) top-to-the-northwest Hercynian event. The Lower Gneiss Unit consists mainly of the Aubazine, Chameyrat–Mulatet and Argentat orthogneisses. The granitoids' host rocks are paragneiss and micaschist derived from greywhacks and shales. In these metasediments the metamorphic assemblages (biotite + garnet ± staurolite ± kyanite ± sillimanite) are attributed to the 360 Ma Hercynian event. The Chameyrat–Mulatet Argentat augen gneiss is dated at 535 ± 21 Ma by the Rb/Sr whole-rock method (Bernard-Griffiths, 1975). Migmatitic facies developed at the expense of the augen gneiss. The con-

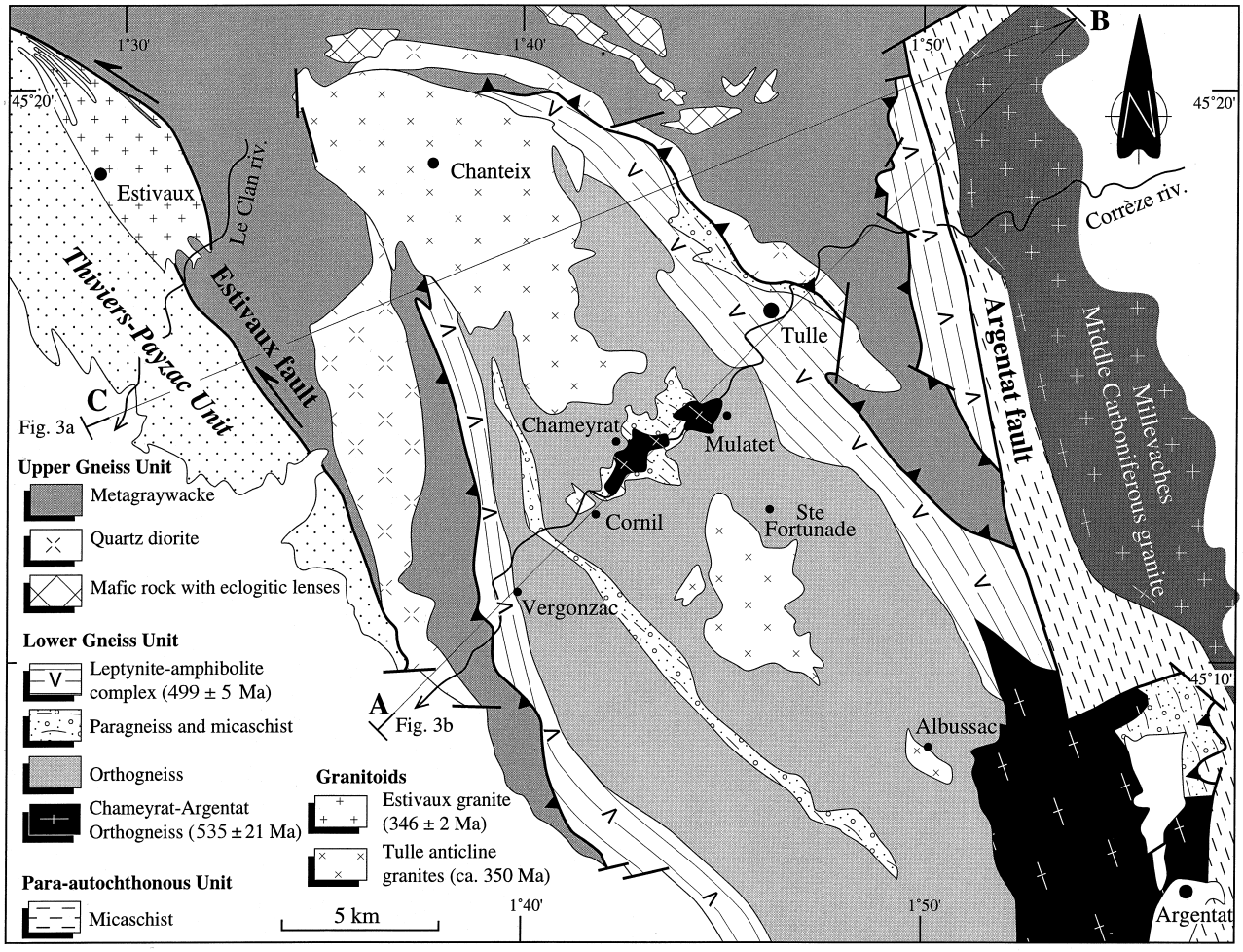

Fig. 2. Geological map of the South Limousin area.

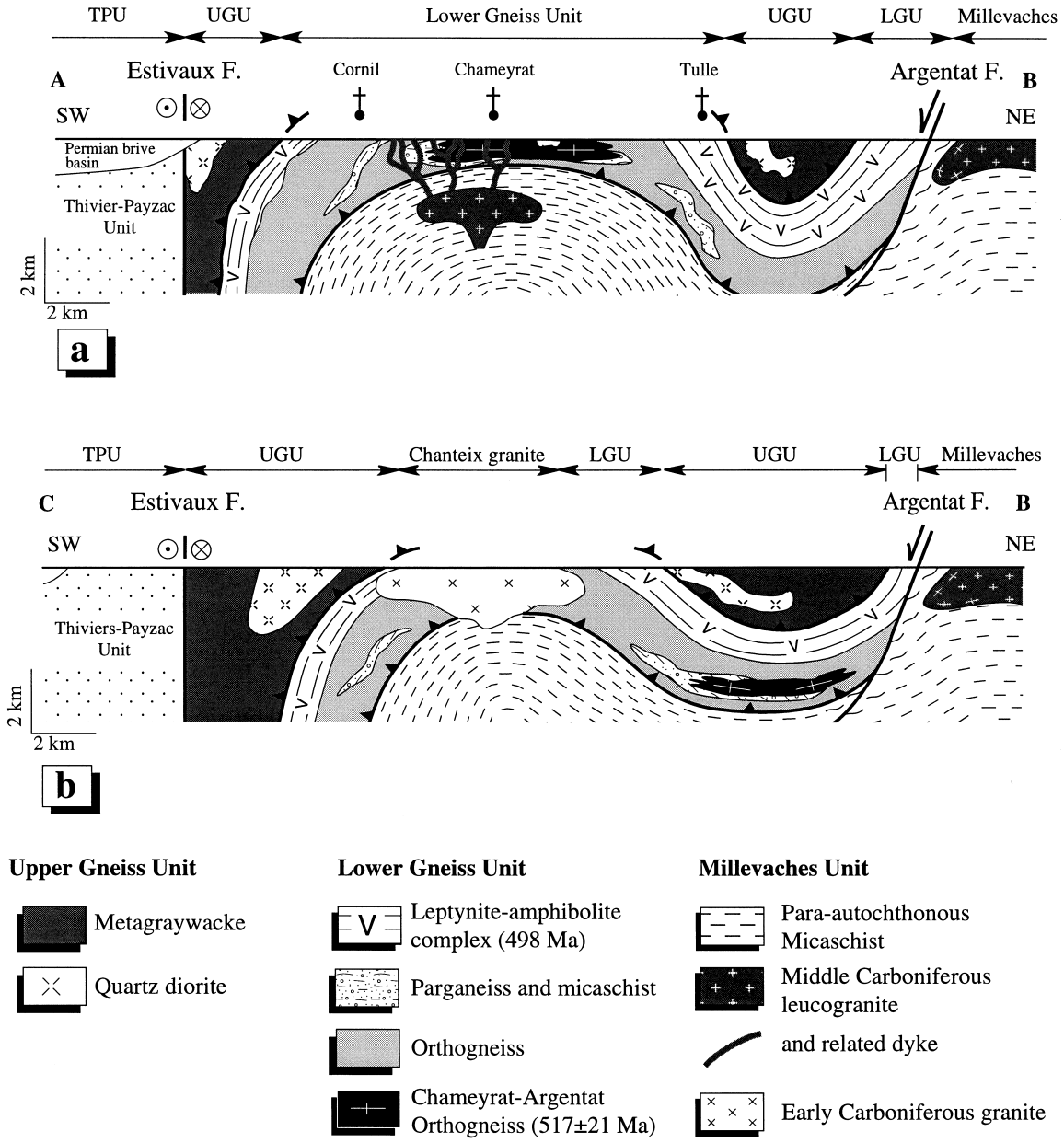

Fig. 3. Geological cross-sections of the Tulle anticline located in Fig. 2. (a) NE–SW cross-section along the Corrèze Valley showing the hidden leucogranitic pluton discussed in the text. (b) NE–SW cross section through the Chanteix pluton.

tact between the Upper Gneiss Unit and the Lower Gneiss Unit is marked by the leptynite–amphibolite complex of Vergonzac–Tulle dated at 499 ± 5 Ma by $^{207}Pb/^{206}Pb$ on zircon (P. Ledru, personal communication). Metashales and metapelites belonging to the Para-autochthonous Unit outcrop only near the Argentat fault. Garnet–biotite assemblages related to the 360 Ma event are retrogressed into white mica and chlorite during the middle Carboniferous extensional tectonics.

The Argentat fault (Figs 2 & 3) is one of the major structures of the French Massif Central (Guillot and Feix, 1985). It separates the Limousin area from the Millevaches area in a N–S direction along 180 km. This fault experienced a polyphase deformation. First, the Argentat fault was a ductile normal-dextral fault acting in the middle Carboniferous times upon already metamorphosed and ductilely deformed micaschists and gneisses (Ledru and Autran, 1987; Mattauer *et al.*, 1988; Roig and Faure, 1996). The Limousin and Millevaches areas represent, respectively, the fault hanging wall and footwall. Although undated, the ductile deformation took place in middle Carboniferous time as numerous leucogranites of this age formed

syn-tectonic plutons. This event corresponds to the first Variscan late-orogenic stage recognized in the Massif Central. Secondly, in late Carboniferous times, the fault zone was reactivated as a brittle, left-lateral strike-slip fault during the second extensional stage (Faure, 1995).

The Tulle anticline is a kilometre-scale, upright antiform located between the Estivaux strike-slip fault to the west and the Argentat fault to the east. This anticline re-folds the metamorphic foliation and the thrust contact between the Upper Gneiss Unit and the Lower Gneiss Unit. Owing to folding, the Chameyrat–Mulatet orthogneiss of the Lower Gneiss Unit crops out in a window along the Corrèze river. In the study area, the subhorizontal axis of the Tulle anticline trends N110°E but turns to N140°E south of Argentat (Guillot, 1981). Our crude estimate indicates an horizontal shortening of 75%. The well-developed antiformal structure along the Corrèze Valley is progressively altered southward by the action of the Argentat fault. Near Sainte-Fortunade the foliation is subhorizontal, and south of Albussac the general structure is a SW-dipping monocline (Fig. 4a & b). The foliation bears a regional lineation subparallel to the Tulle fold axis (Fig. 4a & c). This lineation is a mineral lineation formed by the crystallization of biotite, muscovite and amphibole. Stretching of quartz and feldspar aggregates along the same trend shows that this lineation is the *X* finite-strain axis. In sections parallel to the NW–SE lineation and perpendicular to the metamorphic foliation (*XZ*-plane of the finite-strain ellipsoid), numerous top-to-the-northwest shear criteria are observed in all the metamorphic rocks of the Tulle anticline. Their significance, relevant to the early Carboniferous regional deformation, will not be discussed here. Moreover, in the Lower Gneiss Unit, and especially in the amphibolite layers of the Vergonzac–Tulle leptynite–amphibolite complex, another N50°E-trending linear structure can be observed. It consists of localized striation associated to preferred crystallization of rare biotite crystals. This linear anisotropy can be defined as a 'high-temperature slickenside' (Fig. 4a) which in the following will be related to the granite emplacement.

The granites of the Tulle antiform

Several calc-alkaline granodiorites occupy the core of the Tulle antiform. Namely, from northwest to southeast, they are the Chanteix, Cornil Sainte-Fortunade and Albussac massifs (Figs 2 & 3). These granites are accompanied by numerous dykes and sills well exposed along the Corrèze Valley. In the main granodioritic bodies, two facies can be distinguished. The microgranular facies is located in the centimetric to decametric dykes and sills of the Corrèze Valley but also in the Chanteix and Sainte-Fortunade granitic bodies. A granular to coarse-grained facies is principally observed in the Albussac pluton. Host-rock xenoliths are frequent but only the largest ones were mapped in the Chanteix body (Fig. 4a). In the main plutons, whatever the facies or the massif, the rock mainly consists of plagioclase, biotite, quartz and orthoclase. The plagioclase is oligoclase zoned from An_{27} in the core to An_{16} in the rim. The biotite belongs to the annite–phlogopite suite. The crystallization sequence determined by microstructures is plagioclase, biotite, quartz and, finally, orthoclase. By comparison with experimental work (Naney, 1983), this sequence allows us to determine a 3–5% (weight) H_2O content in the magma for 2 kbar. Zircon, allanite and sphene are also observed but in small quantities. On the basis of petrology, the magma crystallized at 2–2.5 kbar, that is 6–8 km depth, or at about 220–300°C, assuming a 37°C km^{-1} thermal gradient in the study area (Guillot, 1981; Floc'h, 1983).

Major element geochemistry (Guillot, 1981) supports a similar origin for all the plutons. Large and well-crystallized allanite attests to rare earth elements (REE) enrichment. Lastly, the initial $^{87}Sr/^{86}Sr$ ratio between 0.7077 and 0.7155 (Bernard-Griffiths and Vachette, 1970; Bernard-Griffiths, 1975) is considered to indicate a mantle origin, with probably some crustal contamination for the Tulle anticline granodioritic magma. The Tulle anticline granodiorites present quite similar mineralogy, whole-rock chemical composition, plagioclase and biotite chemistry, and zircon typology (Alinat, 1975) with the Estivaux pluton which provided a 346 ± 2 Ma age by $^{40}Ar/^{39}Ar$ method on biotite interpreted as the cooling age (Roig *et al.*, 1996). A previous Rb/Sr date of 334 ± 14 Ma for the Cornil granite is very debatable (Bernard-Griffiths, 1975; recalculated with $\lambda = 1.42 \times 10^{-11}$). According to this author, the Rb/Sr measurements of the Cornil granite (*s.s*) do not allow one to draw an isochron because the alignment is inferred from the addition of an unfoliated leucrocratic dyke interpreted here as a late feature (cf. below). Recent $^{40}Ar/^{39}Ar$ dates on biotite for the Chanteix and Albussac plutons are 355 ± 4 and 351 ± 5 Ma, respectively (Roig, 1997). The granite emplacement age is considered to be *ca* 350 Ma as the plutons were emplaced within country rocks that were at a temperature of 250–300°C, that is below the biotite closure temperature.

STRUCTURE OF THE TULLE ANTICLINE GRANITES

Mesoscale structures

The Tulle anticline granites are accompanied by numerous dykes and sills that outcrop along the Corrèze Valley. Two generations of dykes can be distinguished. The first one consists of grey, ductilely deformed granodiorite. These dykes are folded or boudinaged (Fig. 5a

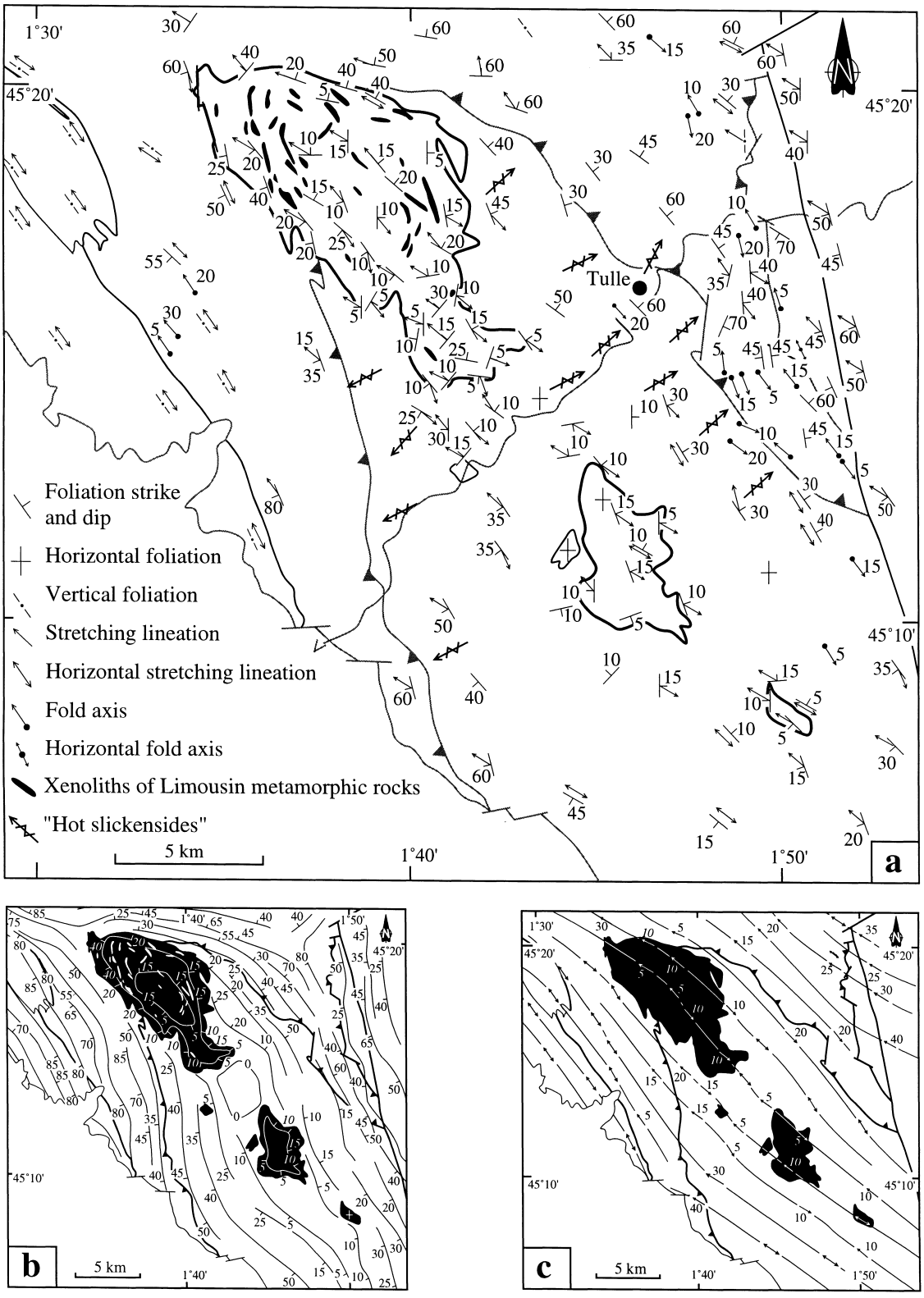

Fig. 4. Structural maps of the South Limousin area: (a) field observations; (b) foliation trajectory; and (c) lineation trajectory.

& b), and contain a well-marked flat-lying solid-state foliation and NW–SE lineation. From the granodioritic composition and deformation features (lineation orientation, microfabric) displayed by these dykes we suggest that they are contemporaneous to the Tulle anticline granodiorites. This first generation of dykes shows a scattering of fold axes without any preferred trend (Fig. 6a). The foliation in the dykes is subhori-

zontal, parallel to host-rock foliation and axial planar. The poles of the dyke walls exhibit a strong N125°E horizontal preferred orientation (Fig. 6b). Because coeval sills are boudinaged in the NW–SE direction (Fig. 5b), these dykes are interpreted as filling cross joints (Marre, 1982; Hibbard and Watters, 1985). This structural pattern allows us to infer a vertical maximum shortening and a NW–SE maximum stretching direction (Z and X-axes of the finite-strain ellipsoid, respectively) during emplacement of the first generation of dykes.

The second generation of dykes consists of pink leucocratic pegmatite and aplite. These latter dykes are neither folded nor foliated. They consistently trend

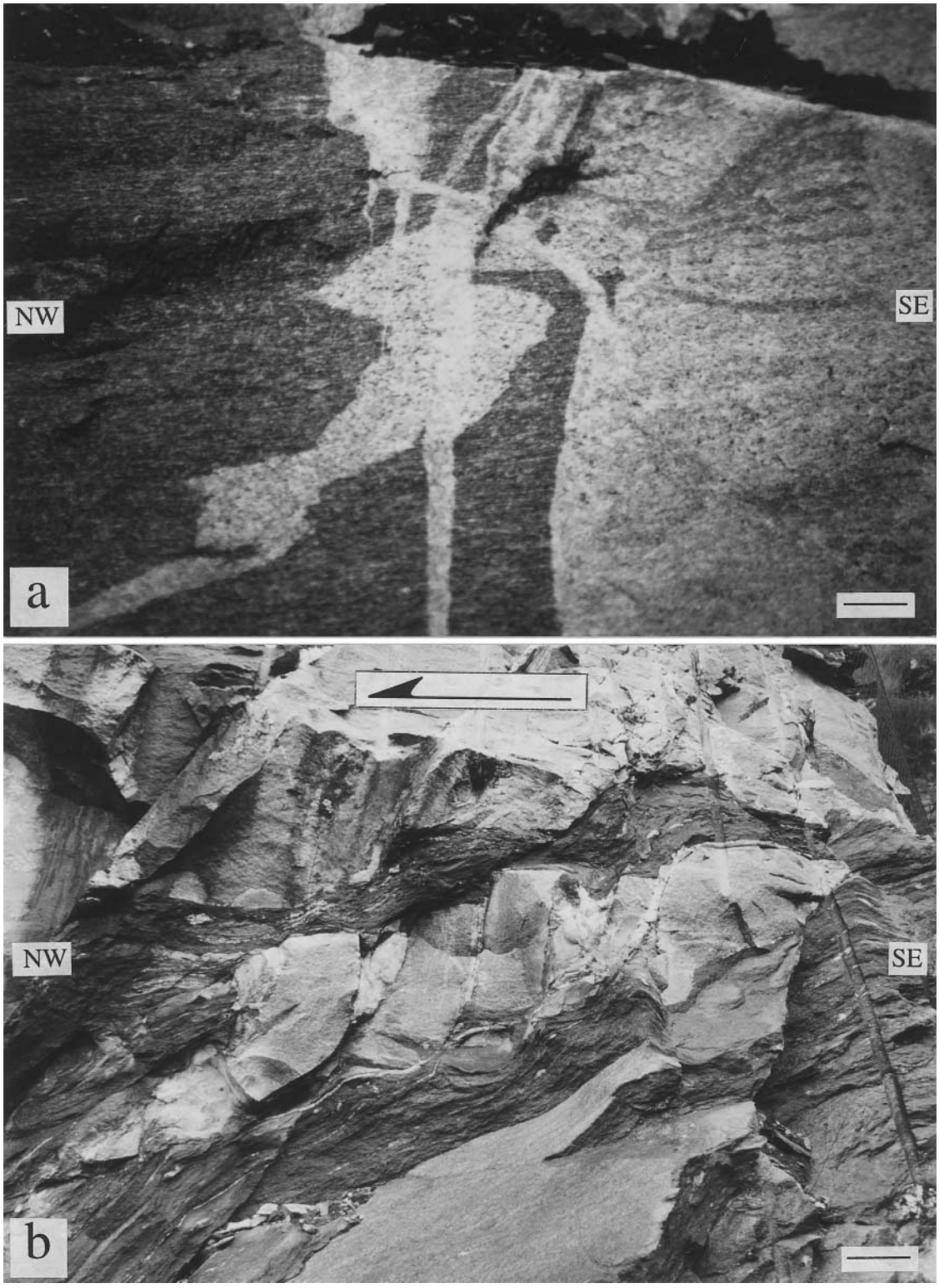

Fig. 5(a & b).

SW–NE (Fig. 6c) and cross-cut the early grey dykes. It is worth noting that such dykes are widespread around middle Carboniferous peraluminous granites in the Massif Central. Dyke swarms do not necessarily indicate the proximity of a pluton, but the presence of these leucogranite dykes and the gravimetric data (cf. below) support the occurrence of a hidden leucogranitic pluton in the core of the Tulle anticline.

In all the Tulle anticline granites, foliation and lineation are well expressed. These planar and linear anisotropies are due both to stretching and to the preferred orientations of the biotite and quartz aggregates, suggesting a post-magmatic fabric of the rock. Host-rock xenoliths are also conformable to the granite crystal fabric (Fig. 4a). However, the occurrence of early magmatic foliation and lineation cannot be ruled out. Near the pluton margins, the granite foliation is always parallel to the contact with the host rock and defines a concentric pattern (Fig. 4b). The lineation in the granitic bodies and in the grey dykes cannot be

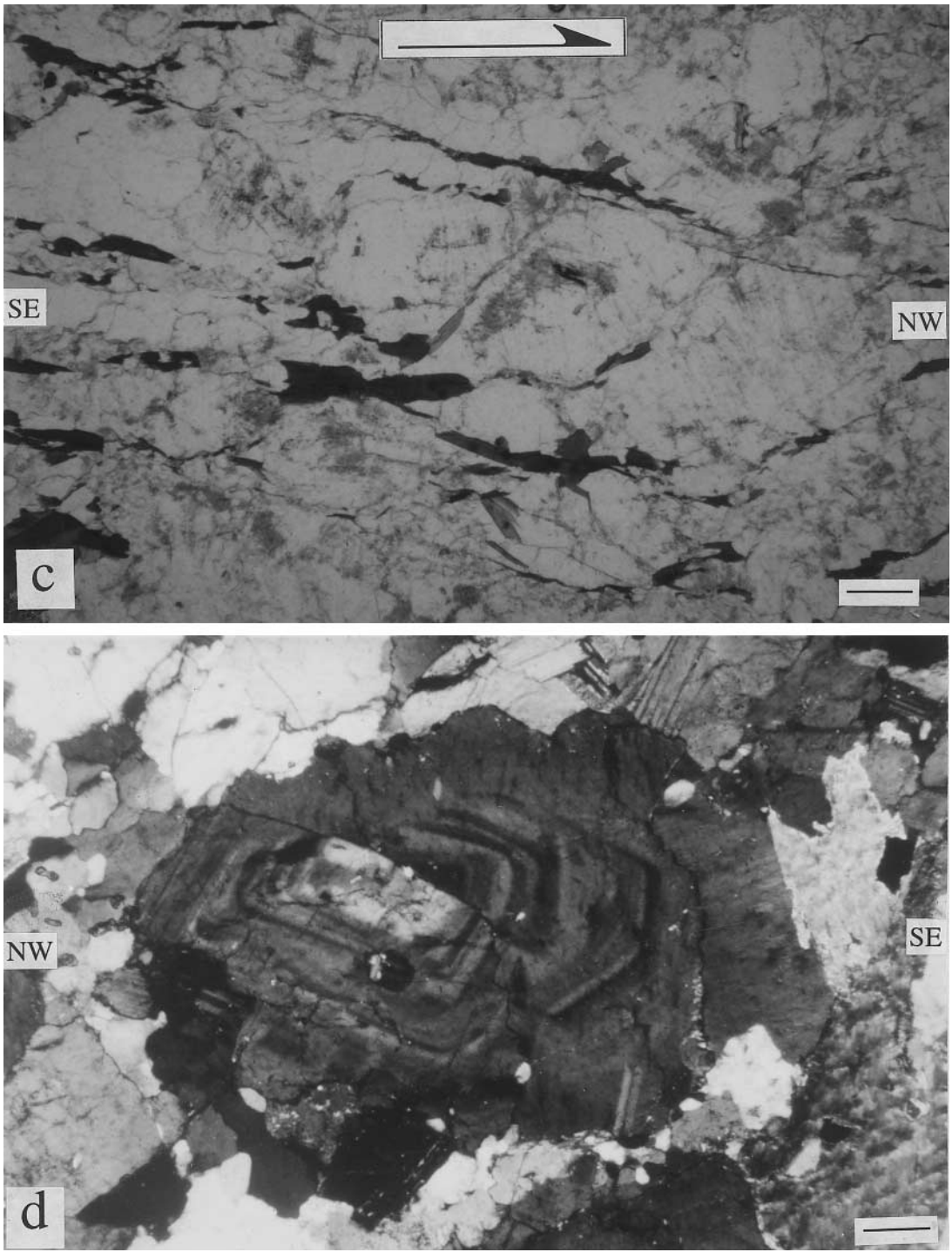

Fig. 5(c & d).

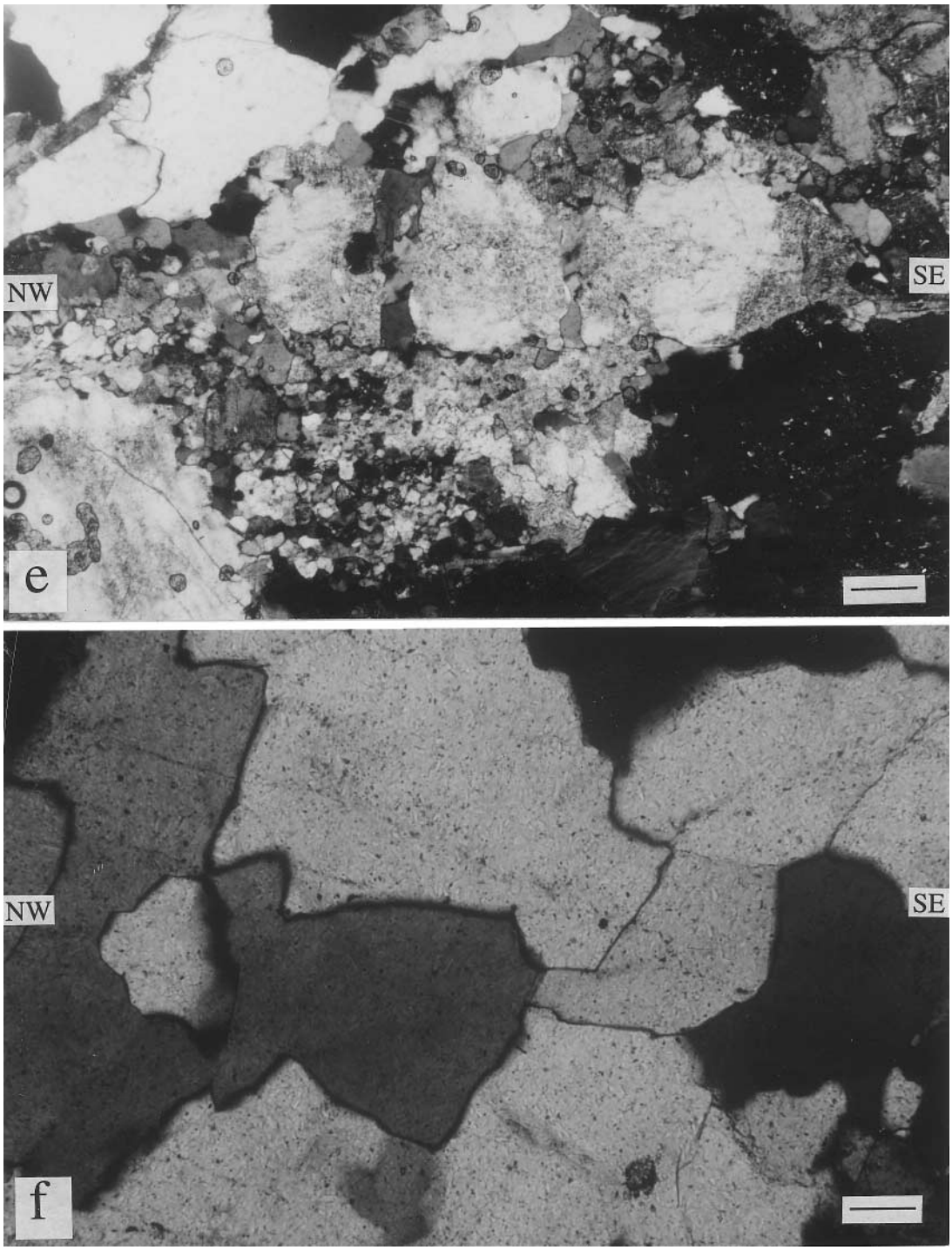

Fig. 5. Examples of the various structures of the Tulle anticline granites. (a) Folded and foliated granodioritic dykes cut by an undeformed leucogranitic dyke. The Corrèze Valley near Cornil. The bar is 10 cm. (b) Asymmetrically boudinaged granodioritic dyke showing top-to-the-northwest shearing. The Corrèze valley near Cornil. The bar is 15 cm. (c) *S–C* structures in the Albussac pluton. The bar is 0.65 mm. (d) Syneusis texture of plagioclase. The Sainte-Fortunade pluton. Crossed polars. The bar is 0.3 mm. (e) Cracked plagioclase with voids filled by infra-millimetric quartz and plagioclase (micro-aplite). The Albussac pluton. Crossed polars. The bar is 0.4 mm. (f) High-temperature quartz with mosaic-like

geometrically separated from that of the host rock. The geometric concordance of the foliation and lineation trends between the host rocks and magmatic rocks indicates that the direction of the finite strain axes remained constant from the regional deformation (*ca* 360 Ma) to pluton emplacement (*ca* 350–340 Ma). The lineation trajectory (Fig. 4c) passes through the Tulle anticline axis and granitic bodies suggesting a structural relationship between folding and fabric development in the plutons.

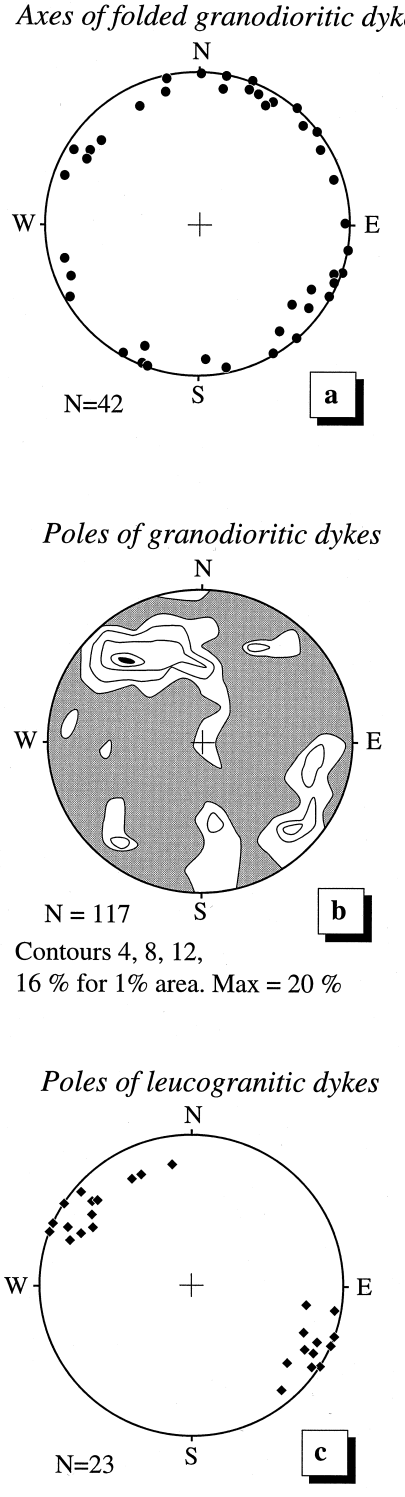

Fig. 6. Stereograms of the dyke structures. (a) Plot of the fold axes of the granodioritic dykes. (b) Density plot of the granodiorite dyke walls interpreted as cross-joints. (c) Poles of the leucogranitic dykes.

Microstructural data

In the inner parts of the Chanteix and Sainte-Fortunade bodies minerals are just preferentially oriented without significant ductile strain, whereas at the northwestern and southeastern borders of the plutons all minerals are plastically deformed. As a whole, in the Chanteix pluton, a grain-size reduction occurs from the centre to the border of the massif. The kinematics deduced from *S–C* structures indicate divergent senses of shear: top-to-the-northwest shear in the northwest border and top-to-the-southeast shear in the southeast border. Metre-scale shear bands observed in grey sills and their host rock confirm this kinematic pattern. However, in the Albussac massif, *S–C* structures developed under solid-state deformation always indicate a top-to-the-northwest shear (Fig. 5c). These data are in agreement with the kinematics inferred from quartz ⟨*c*⟩-axis preferred orientations, presented further on.

In all the granites, oriented plagioclase crystals and magmatic texture such as syneusis (Fig. 5d) are often observed, indicating that the early stages of fabric development were coeval to magma crystallization (Paterson *et al.*, 1989). Frequently, plagioclase is also cracked perpendicular to the stretching lineation, and voids are filled by infra-millimetric orthoclase, sodic plagioclase and quartz (Fig. 5d). This association of very small quartz and feldspar crystals was previously described as micro-aplite (Hibbard, 1986). Micro-aplite is also found in the continuation of plagioclase crystals along the stretching direction. This melt relocation texture can be interpreted as a pressure shadow. In our samples, myrmekites are observed in the plane perpendicular to the foliation and parallel to the stretching direction (*XZ*-plane). The significance of myrmekites is ambiguous because they can be found either in metamorphic rocks, formed in the solid-state, or in igneous rocks with melt participation (Hibbard, 1979; Simpson and Wintsch, 1989; Vernon, 1991). However, in our case, myrmekites present a mantle-like texture adjacent to feldspars that is considered a typical texture of fluid relocation (Hibbard, 1979). The myrmekite mantle-like texture and the fact that micro-aplite appears around and in the plagioclase micro-fractures is evidence for melt relocation during the last stages of granite crystallization under dynamic conditions (Hibbard, 1986; Bouchez *et al.*, 1992; Roig *et al.*, 1996). When granites are emplaced during regional deformation, the last fraction of magma will migrate and crystallize in the low-strain domains such as cracks formed by brittle fracturing of already crystallized crystals or in the strain shadows around crystals. All these textural observations indicate a pre-full crystallization deformation and support the interpretation that the Tulle anticline granodiorites are syn-kinematic bodies.

Fabric analyses

Owing to the lack of mafic enclaves, rock fabrics were computed at the microscopic scale in order to get information on finite strain using two different methods. (i) The R_f/Φ method (Ramsay, 1967; Dunnet, 1969) was applied on quartz aggregates. The lengths of long and short axes and the orientation of the long

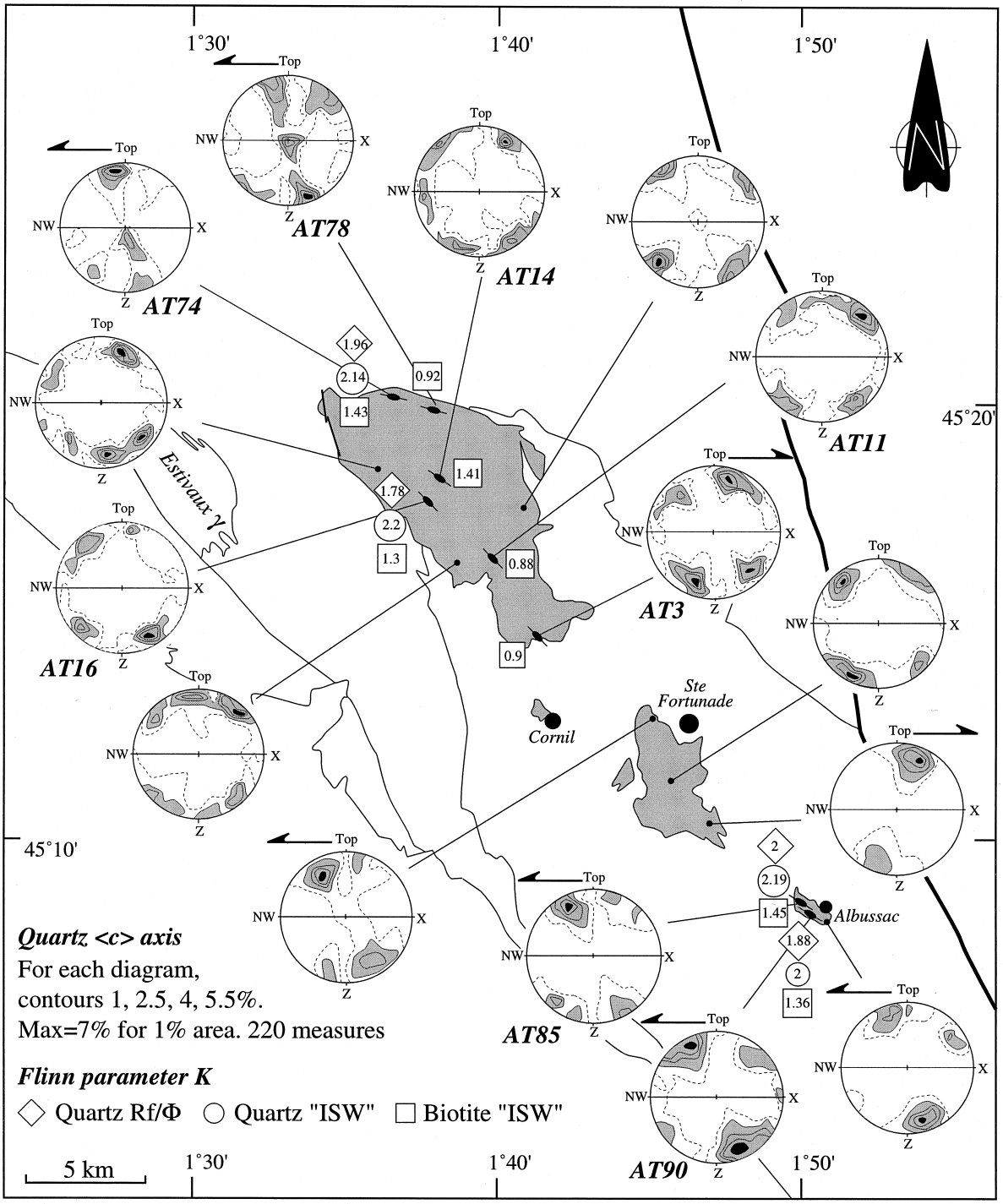

Fig. 7. Quartz ⟨*c*⟩-axis petrofabrics and strain measurements of the Tulle anticline granites. Numbers are the Flinn parameter *K*.

axis of the bulk quartz aggregates were determined by image analysis. Large quartz aggregates are only found in the coarse-grained facies which is poorly represented and only four samples were analysed by the R_f/Φ method. Two of them come from the Chanteix granite (AT16 and AT74) and two from the Albussac granite (AT90 and AT85, Fig. 7). (ii) A technique derived from the 'inverse SURFOR wheel' method (Panozzo, 1987) was also used. This method consists of rotating a set of parallel lines of fixed and constant length through 180° and counting the intersections with the drawing of the fabric outline at regular angle intervals, φ. The number of intersections, n, is plotted as a function of the orientation φ. A curve is fitted through the points. The ratio $n(\varphi)_{max}/n(\varphi)_{min}$ corresponds to the ratio of the maximum and minimum axes of the strain ellipse. This method is classically used for outlines of grain boundaries (Panozzo, 1987; Lagarde *et al.*,

Table 1. Characteristics of the ellipsoids calculated with different methods (see Fig. 8)

	■ Biotite 'ISW'			● Quartz 'ISW'			◆ Quartz R_f/Φ		
	Y/Z	X/Y	K	Y/Z	X/Y	K	Y/Z	X/Y	K
AT85	1.38	1.55	1.45	1.32	1.7	2.19	1.66	2.32	2
AT90	1.45	1.61	1.36	1.32	1.64	2	1.58	2.09	1.88
AT74	1.42	1.6	1.43	1.36	1.77	2.14	1.49	1.96	1.96
AT16	1.33	1.43	1.3	1.3	1.66	2.2	1.45	1.8	1.78
AT78	1.52	1.48	0.92						
AT14	1.32	1.45	1.41						
AT11	1.42	1.37	0.88						
AT3	1.41	1.37	0.9						

ISW, 'inverse SURFOR wheel' method (Panozzo, 1987)

1994). In our case, we used this method for biotites and quartz aggregates.

In the Chanteix pluton, sample AT74 shows *S–C* planes and dynamic recrystallization of quartz, but sample AT16 in the pluton centre is weakly deformed as the quartz texture does not exhibit dynamic recrystallization. The samples from the Albussac body (AT90 and AT85) show *S–C* planes defined by biotite, and quartz grains present dynamic recrystallization texture. Therefore, except in the core of the Chanteix Massif, the foliation and lineation in the Tulle anticline plutons are mostly due to solid-state deformation.

The 'inverse SURFOR wheel' method was also used on these four samples. Nevertheless, in order to better describe the fabric ellipsoid, the 'inverse SURFOR wheel' method on biotite aggregates was used for four other samples of micro-granular facies from the Chanteix body (AT3, AT11, AT14, AT78, Fig. 7). The reliability of the techniques used requires an important number of measurements. Thus, three *XZ* and *YZ* sections were cut in each sample for measurements. The stretching lineation and the foliation are considered to represent the *X*-axis and *XZ*-plane of the finite strain ellipsoid, respectively. In the Tulle anticline granites, due to dynamic recrystallization, quartz grains do not act as perfect passive markers. Moreover, because of the internal anisotropy and viscosity contrast between grains, strain estimates are only semi-quantitative. The results are displayed in Table 1.

The Flinn plot (Fig. 8) shows that quartz and biotite behaved differently. Quartz clusters can be approximated as passive markers, even if their initial shape is partly controlled by the framework constituted by early crystallizing minerals. Thus, the quartz shape fabric is closer to the bulk strain ellipsoid than the biotite preferred orientation. The biotite grains are first oriented during their crystallization from the magma. The primary planar fabric will influence the final shape fabric and give lower values of the Flinn parameter. In addition, biotite will crystallize all along the deformation history of the plutons. Biotite grains in *S*-planes could be considered as relicts of early magmatic crystals, partly recrystallized during deformation, while those in the *C*-planes could be interpreted as late post-magmatic crystals. Therefore, an inherited component of strain is incorporated in our estimate from biotite. This phenomenon may account for the systematically lower *K* values obtained for biotite. The calculated ellipsoids from quartz aggregates fall in the constrictional field ($K = 2$) whatever the rock facies or the method used (Fig. 8).

Our fabric measurements of the Tulle anticline granites show that the *Y*-axis of the finite-strain ellipsoid is a shortening direction which is horizontal and also perpendicular to the fold-axial plane. Such a constrictional strain is in agreement with the creation of a large-scale upright open fold. Thus, folding of the host rock appears to have occurred during or slightly after granite emplacement as solid-state fabrics are weakly developed in the internal parts of the plutons. The relationships between the formation of the Tulle antiform and pluton emplacement will be further discussed after the presentation of the gravity modelling.

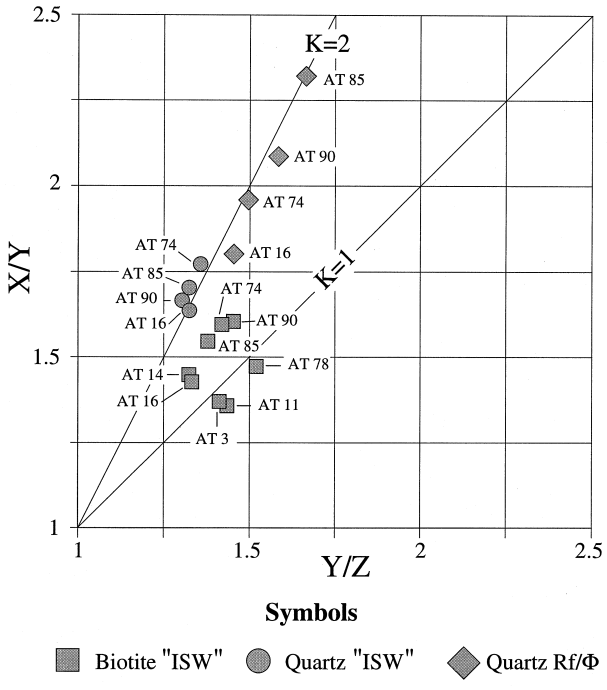

Fig. 8. Flinn diagram of the calculated ellipsoids. ISW, 'inverse SURFOR wheel' method (Panozzo, 1987).

Quartz ⟨c⟩-axis preferred orientations

In the granular facies, large polycrystalline quartz aggregates are elongated in the maximum principal finite stretch direction. Within the aggregate, the quartz grains often show lobed boundaries which give a puzzle-like texture. The grain boundaries also have straight contours forming a mosaic-like texture (Fig. 5f). This texture is interpreted to indicate a high-temperature deformation (Lister and Dornsiepen, 1982; Gapais and Barbarin, 1986). In the micro-granular facies aggregates are not found; quartz only occurs as single crystals. In both facies, quartz grains have undulose extinction and the few subgrains observed show that the dynamic recrystallization is relatively weak. In the Chanteix and Sainte-Fortunade granodiorites, the quartz ⟨c⟩-axis preferred orientation has an orthorhombic symmetry with respect to the foliation plane, except for the northern and southern parts of the massifs (Fig. 7). In the Albussac body, the fabrics are asymmetric with respect to the foliation plane. The monoclinic fabrics are characterized either by a point maximum on the edge of the diagram (Albussac and Sainte-Fortunade massifs), an oblique girdle or two asymmetric crossed-girdles with respect to the foliation pole (Chanteix body). Assuming intracrystalline glide as the active deformation mechanism, basal ⟨a⟩ and to a lesser extent prismatic ⟨a⟩ slip systems indicative of a low to medium temperature are responsible for this fabric development (Lister and Hobbs, 1980; Jessell and Lister, 1990). The monoclinic symmetry allows us to infer a non-coaxial deformation (Lister and Hobbs, 1980; Etchecopar and Vasseur, 1987; Law, 1990). In agreement with other shear criteria such as *S–C* structure (Fig. 5c), the kinematics deduced from these ⟨c⟩-axis fabrics show: (i) a top-to-the-northwest shear for the Albussac massif; and (ii) divergent senses of motion for the Chanteix and Sainte-Fortunade bodies: top-to-the-northwest in the northwestern part and top-to-the-southeast in the southeastern part of the bodies (Fig. 7).

In the centres of the Chanteix and Sainte-Fortunade massifs, the fabrics are symmetric with respect to the foliation pole and the maxima are located on the edge of the diagram (Fig. 7). According to natural examples and numerical modelling, such orthorhombic fabrics are explained by a coaxial strain regime (Etchecopar, 1977; Lister and Hobbs, 1980; Lister and Dornsiepen, 1982; Law, 1987). In terms of kinematics, the symmetry of quartz ⟨c⟩-axis diagrams of the Tulle anticline granites could result from a coaxial flow regime accommodated by basal ⟨a⟩ slip. However, the quartz deformation mechanism responsible for the symmetrical fabrics is debated. Maxima formed during non-coaxial flow are due to activation of a dominant slip system in the most favourable direction for gliding. In contrast, fabric maxima due to coaxial strain are related to the activation of two or three different easy-to-activate glide systems symmetrically disposed with respect to the shortening axis. On the orthorhombic stereograms (Fig. 7), the maxima located on the edge of the diagram correspond to the maximum III of Lister and Dornsiepen (1982). These authors suggest maximum III might arise because of activation of trigonal dipyramidal $\{2\bar{1}\bar{1}2\}$ ⟨c + a⟩ systems at high temperature ($T > 700^{\circ}$C). Our orthorhombic fabrics may result from coaxial deformation accommodated by basal ⟨a⟩ glide. The mosaic texture observed in some thin sections suggests a high-temperature deformation that would not be compatible with the activation of the basal ⟨a⟩ gliding system. In that case, ⟨c⟩-axis maxima close to the lineation direction, characteristic of prism ⟨c⟩ slip, would be expected. Such fabrics are recognized in high-temperature deformed rocks such as migmatites and granites (e.g. Bouchez *et al.*, 1985; Blumenfeld *et al.*, 1985; Gapais and Barbarin, 1986; Mainprice *et al.*, 1986; Tommasi *et al.*, 1994; Roig and Faure, 1995). One explanation for the presence of the locally developed mosaic texture might be a limited static recrystallization (annealing) caused by a late reheating of the Tulle anticline granites, during emplacement of the hidden pluton modelled further on. However, the lack of high-temperature textures in the micro-granular facies and TEM observations allow us to argue the mosaic textures pre-date development of the orthorhombic ⟨c⟩-axis fabrics.

TEM analysis

We chose a limited number of samples representative of the question to be solved: "What is (are) the mechanism(s) responsible for the development of apparently low-temperature quartz ⟨c⟩-axis fabric and high-temperature quartz textures?" Sample AT74 was selected because it clearly shows quartz mosaic-like texture (Fig. 5f) and basal to prismatic ⟨a⟩ operative slip system (Fig. 9). TEM observations were made on several individual quartz grains containing well-defined subgrain boundaries (SGB). All observations were carried out with Prof. J. C. Doukhan on a Philips CM30 STEM in the Laboratoire de Structures et Proprietés de l'Etat Solide, Université Lille 1, France.

The samples were ion thinned and carbon-coated for TEM observations of free dislocations and SGBs. In order to identify the dislocations, the technique of 'invisibility criteria' was used (Hirsh *et al.*, 1965; Ardell *et al.*, 1974; Trépied *et al.*, 1980). For a dislocation to be out of contrast requires the following conditions: the dot product $\vec{\mathbf{b}}\cdot\vec{\mathbf{g}} = 0$ (1) for a pure screw dislocation and $\vec{\mathbf{b}}\cdot\ \vec{\mathbf{g}}\times\vec{\mathbf{u}} = 0$ (2) for a pure edge dislocation, where $\vec{\mathbf{g}}$ is the diffraction vector, $\vec{\mathbf{b}}$ the Burgers vector and $\vec{\mathbf{u}}$ the unit vector along the dislocation line. All the samples studied show the same features. The study of free dislocations allows us to evaluate an average dislocation density of about $\rho = 6\times10^{12}$ m^{-2}. The observed

dislocations often form junctions, and very few dislocation loops are observed. The pictures of the same area with two different diffraction vectors, $\vec{\mathbf{g}} = [1\bar{1}0\bar{1}]$ and $\vec{\mathbf{g}} = [1\bar{1}00]$, are quite identical (Fig. 9a & b). This precludes the occurrence of $\langle c \rangle$-type dislocations. Furthermore, these pictures show that all the free dislocations are $\langle a \rangle$-type. These free dislocations are in climb configuration and the numerous junctions allow us to infer a medium temperature for their occurrence. These free dislocations reveal that the basal $\langle a \rangle$ and, to a lesser extent, the prismatic $\langle a \rangle$ gliding systems were operative. Thus, a temperature of about 300–400°C is in agreement with the quartz $\langle c \rangle$-axis fabrics (Fig. 7).

Subgrain boundaries parallel to $[01\bar{1}0]$ with a diffraction vector $\vec{\mathbf{g}}$ dislocations = $[01\bar{1}1]$ are rare (Fig. 9c) and fluid inclusions are never found in these SGBs. The three sets of $\langle a \rangle$ dislocations (Fig. 9c) confirm the activation of basal $\langle a \rangle$ glide system. Nevertheless, most of the observed SGBs are well organized, show a lot of fluid inclusions and are parallel or slightly oblique with respect to [0001] (Fig. 9d). They are in equilibrium configuration and can be composed of $\langle c \rangle$ dislo-

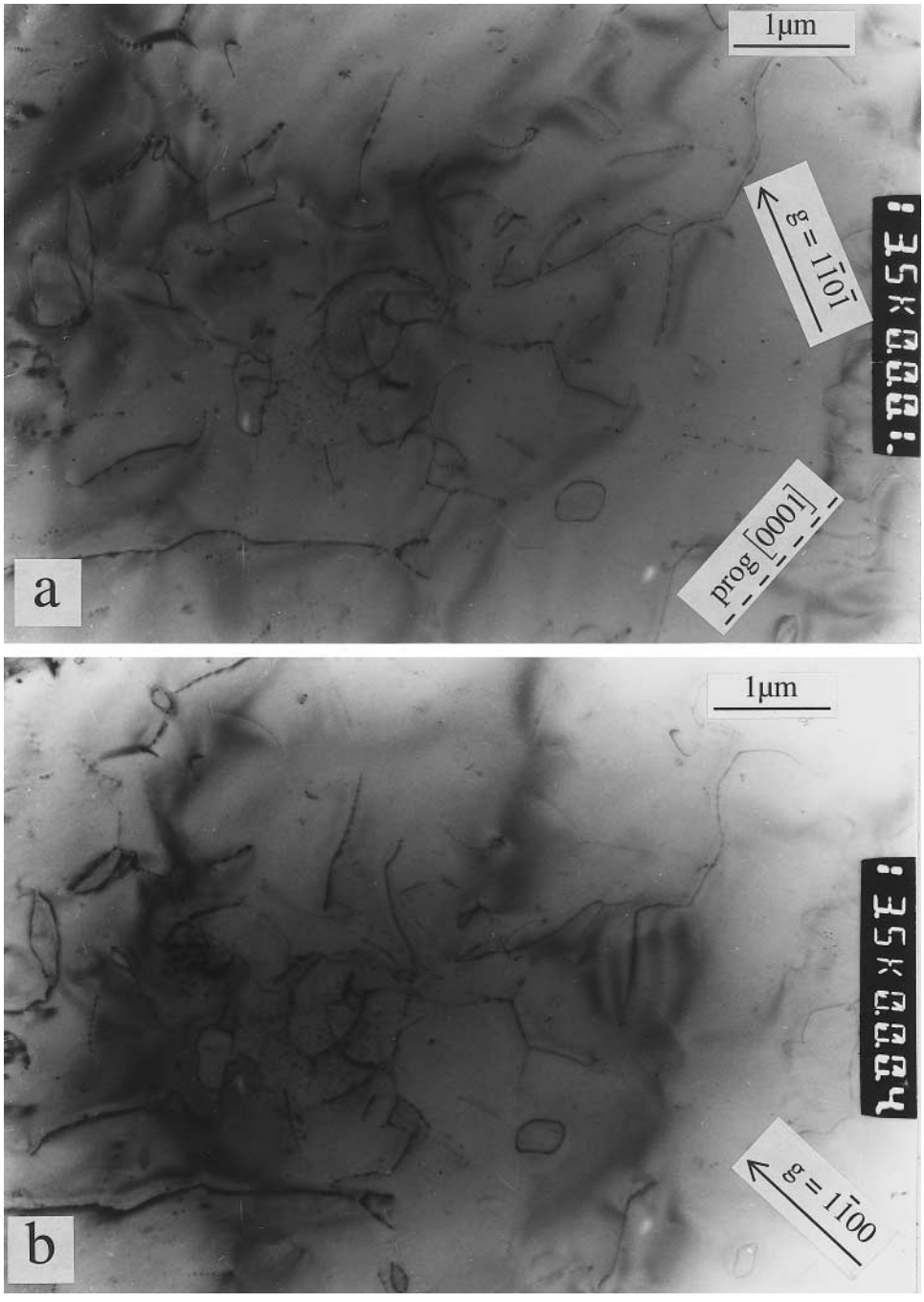

Fig. 9(a & b).

cations. The bright and dark field images of the dislocations in such a SGB are shown in Fig. 9(d–f). Figure 9(f) is an enlarged view of the Fig. 9(e). The small bright lines forming this SGB are ⟨*c*⟩ dislocations. The choice of a diffraction vector ($\vec{\mathbf{g}} = [1\bar{1}01]$) puts them in contrast, while dislocations with Burgers vector $\vec{\mathbf{b}} = 1/3\ [11\bar{2}0]$ are out of contrast. The ⟨*c*⟩ dislocations cannot be out of contrast contrary to the ⟨*a*⟩ dislocations (Fig. 9e & f). Thus, the dislocations forming SGBs are mainly ⟨*c*⟩ dislocations. The activation of the prismatic ⟨*c*⟩ gliding system occurs around 600°C and higher. The occurrence of Dauphiné twins is also indicative of this temperature (Fig. 9c).

TEM analyses allow us to infer an evolution of the quartz deformation in the Tulle anticline granites from a high-temperature deformation regime to a regime at lower temperature. The first event corresponds to a high-temperature (600–650°C) deformation controlled by crystal plasticity *s.s.* In spite of high-temperature conditions, TEM observations rule out diffusion-controlled oriented grain growth as the main deformation mechanism. The high-temperature event is responsible

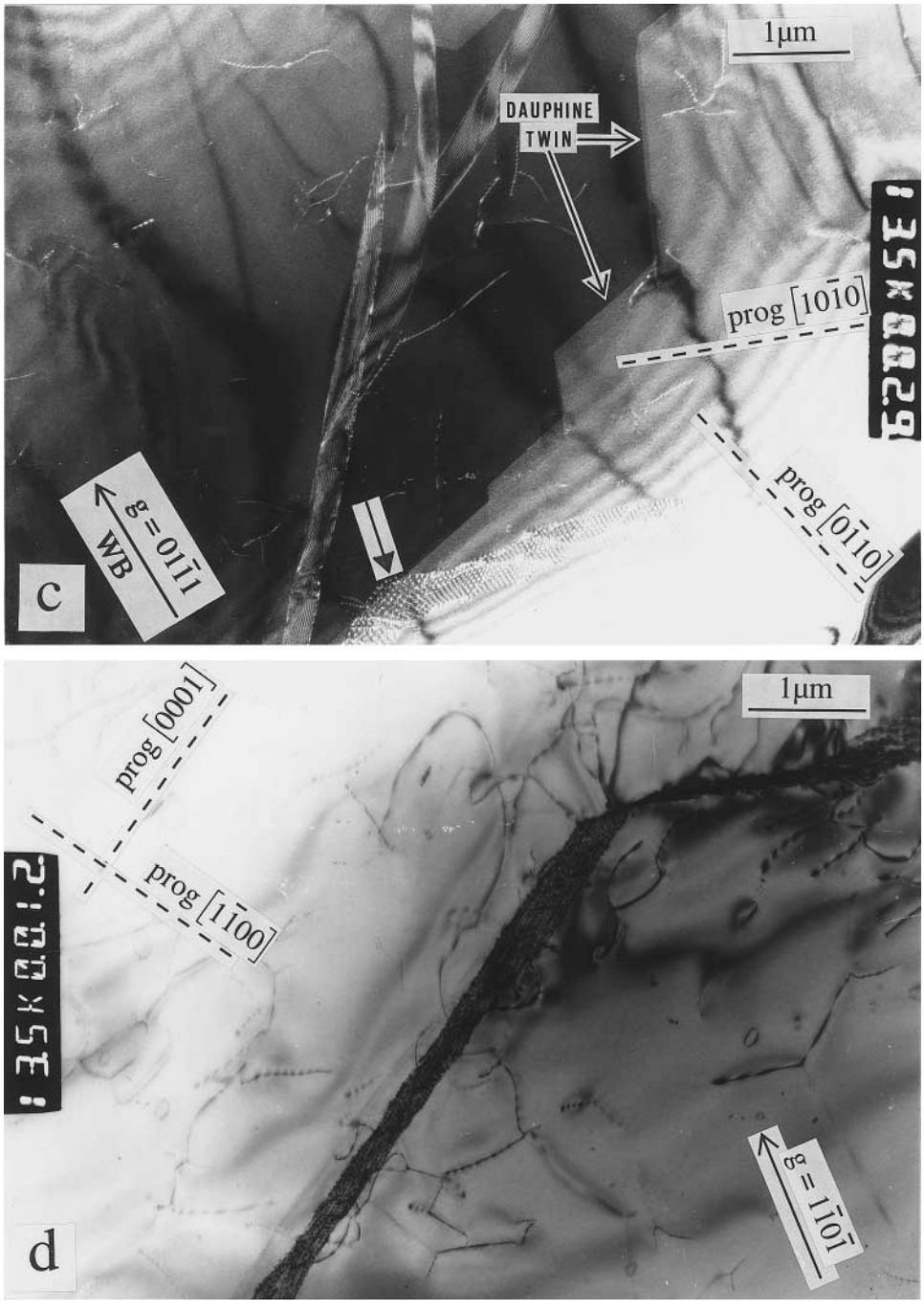

Fig. 9(c & d).

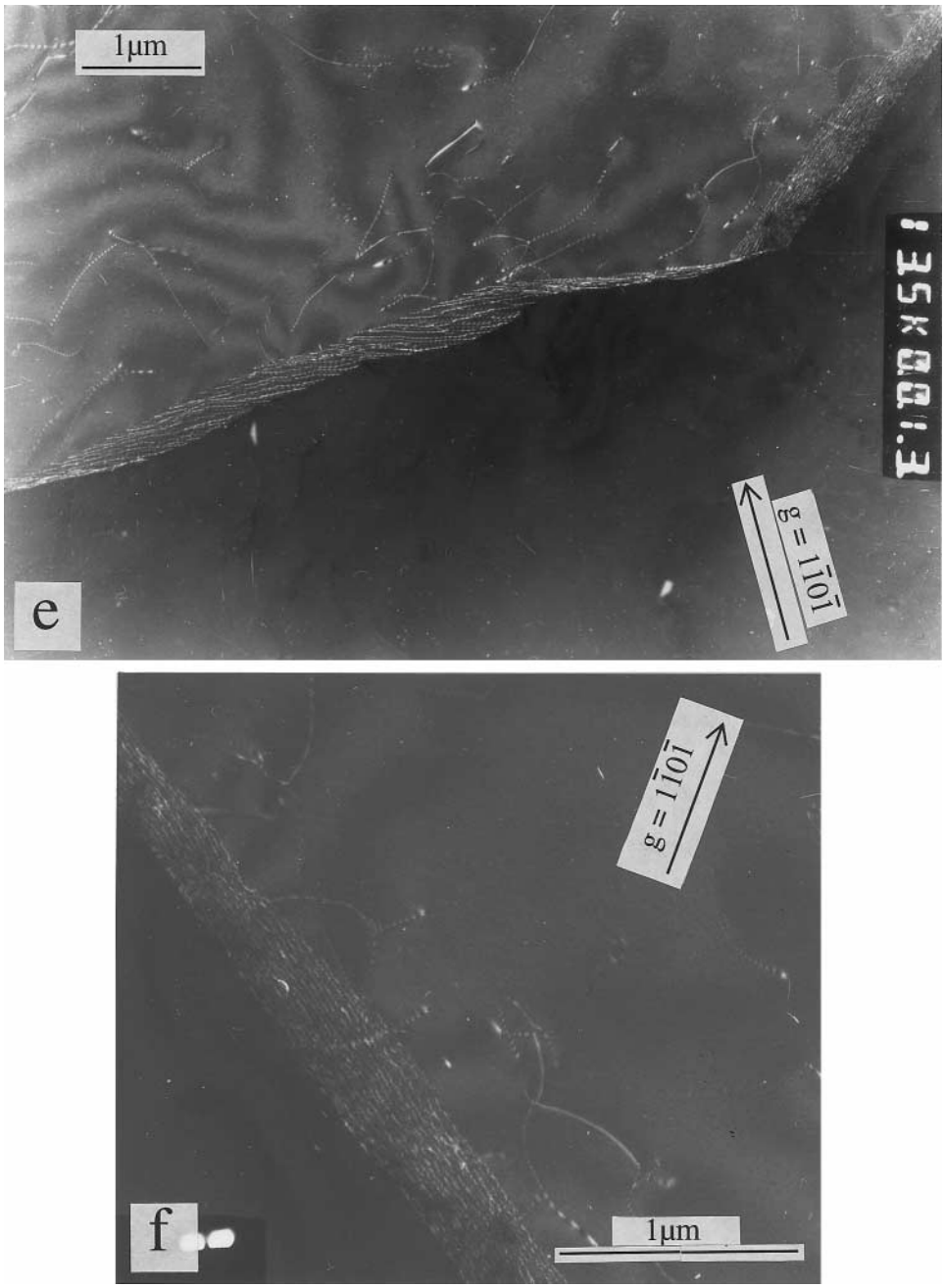

Fig. 9. TEM photographs of quartz structures. (a & b) Bright field of ⟨*a*⟩-type free dislocations with two different diffraction vectors (see text for further information). (c) Dark field weak beam picture of Dauphiné twin and SGB. Note the occurrence of three families of ⟨*a*⟩ dislocations forming the SGB (dark arrow). (d) Bright field of a SGB parallel to the [0001]. (e) Dark field weak beam picture of the same SGB. The comparison between (d) and (e) allows us to identify ⟨*c*⟩-type dislocations (see text for further information). (f) Enlarged view of (e).

for Dauphiné twins, activation of prism ⟨*c*⟩ slip and creation of SGBs, mostly constituted of ⟨*c*⟩ edge dislocations, giving rise to the mosaic-like texture. This deformation mechanism was certainly enhanced by dissolved water. During the pluton cooling, temperature dropped and water precipitated in the SGBs. Then at low temperature (350–400°C), the activated gliding systems were basal (±prismatic) ⟨*a*⟩, with formation of a few ⟨*a*⟩ SGBs. This late deformation event produced enough plasticity to induce the observed ⟨*c*⟩-axis fabrics, but locally permitted the good preservation of the high-temperature mosaic-like texture.

GRAVITY MODELLING

Foliation and lineation patterns provide insufficient information to determine an accurate three-dimensional shape of a granitic pluton, thus the use of gravimetry is essential, although interpretations are not always unique. The Bouguer anomaly gravimetric map shows a strong contrast between areas of different densities corresponding to the Upper Gneiss Unit and Lower Gneiss Unit, respectively (Fig. 10). The Tulle anticline granites do not correspond to a significant negative anomaly. However, along the Corrèze Valley,

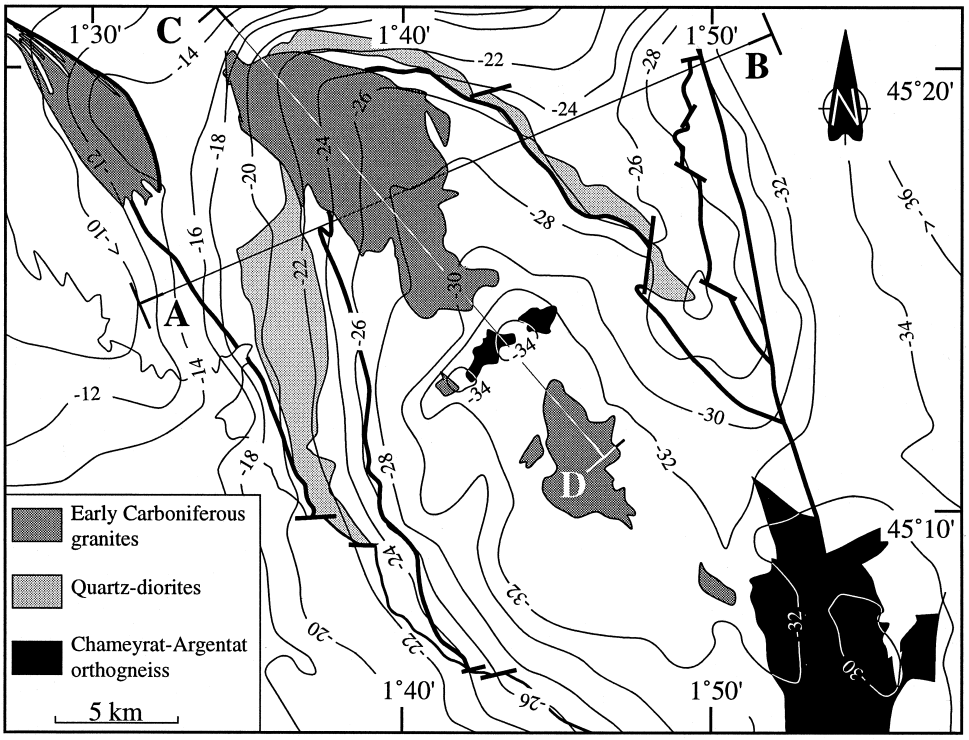

Fig. 10. Bouguer anomaly map of the Tulle anticline area.

two subcircular negative anomalies are observed. It is worth noting that these minima are exactly located in the outcrop area of the pink leucogranite dykes. Therefore, we interpret the Corrèze Valley anomaly as due to a hidden leucogranite pluton linked to the dykes (Fig. 3). The gravity contrast between the Upper Gneiss Unit and Lower Gneiss Unit is due to the quartz-diorites, amphibolites and eclogites of the Upper Gneiss Unit. No significant density difference exists between the paragneiss of the Upper Gneiss Unit and the metagranite and micaschists of the Lower Gneiss Unit. In order to simplify the modelling, a mean density average of both paragneiss and orthogneiss of the Lower and Upper Gneiss Units was calculated. Nevertheless, because of the heterogeneity of these two units, the calculated density average is only an estimate. Locally, the true density can be lower or higher than the calculated one. Moreover, the density contrast between the Tulle anticline granodiorites and their host rocks is sometimes insufficient for a 2.5-dimensional modelling. This is especially true for the small Sainte-Fortunade and Albussac massifs (Fig. 10). Therefore, only two cross-sections of the Chanteix body parallel and perpendicular to structures were modelled using the 2.5-dimensional modelling method (Plouff, 1975) with GMI-PACK software (BRGM-Total) at BRGM (Orléans, France). The half-dimension corresponds to the cartographic extension of the pluton. For the transverse SW–NE cross-section, the modelled gravimetric anomaly curve across the Tulle antiform and the Chanteix pluton fits well with the measured anomaly curve (Fig. 11a). Because of the heterogeneous density of the Upper Gneiss Unit, a mass shortage appears on the northwest border of the longitudinal SE–NW cross-section (Fig. 11b). A test was carried out with continuous quartz-diorite under the Chanteix Massif but the anomaly generated was not large enough to fill the mass shortage. Another test was made with eclogite, but the thickness necessary to fit the curve was too important. This heavy anomaly could be explained by a superimposition of quartz-diorites and eclogites, but their respective thickness is too hypothetical. For this reason no heavy body was represented below the Chanteix pluton. The NW–SE gravimetric cross-section allows us to represent the hypothetical low-density body responsible for the negative anomaly of the Corrèze valley (Fig. 11b). Obviously the Chameyrat orthogneiss cannot be responsible for the anomaly as it has almost the same density as the host rock. Indeed, the Argentat orthogneiss, which is similar to the Chameyrat one, does not produce a negative anomaly. Therefore, the negative anomaly is best explained by the occurrence of a hidden low-density body. In order to estimate its thickness, and its depth, the thickness of the Chanteix pluton was fixed according to the SW–NE cross-section (Fig. 3b). The gravimetric anomaly curve corresponding to modelled cross-section of both the Chanteix and the hidden body fit well with the measured anomaly curve except at its northwestern end for the density reasons discussed above. Modelling that does not take into account the hidden pluton does not fit the real anomaly curve (Fig. 11b). As already stated, dyke petrology and former Rb/Sr results argue

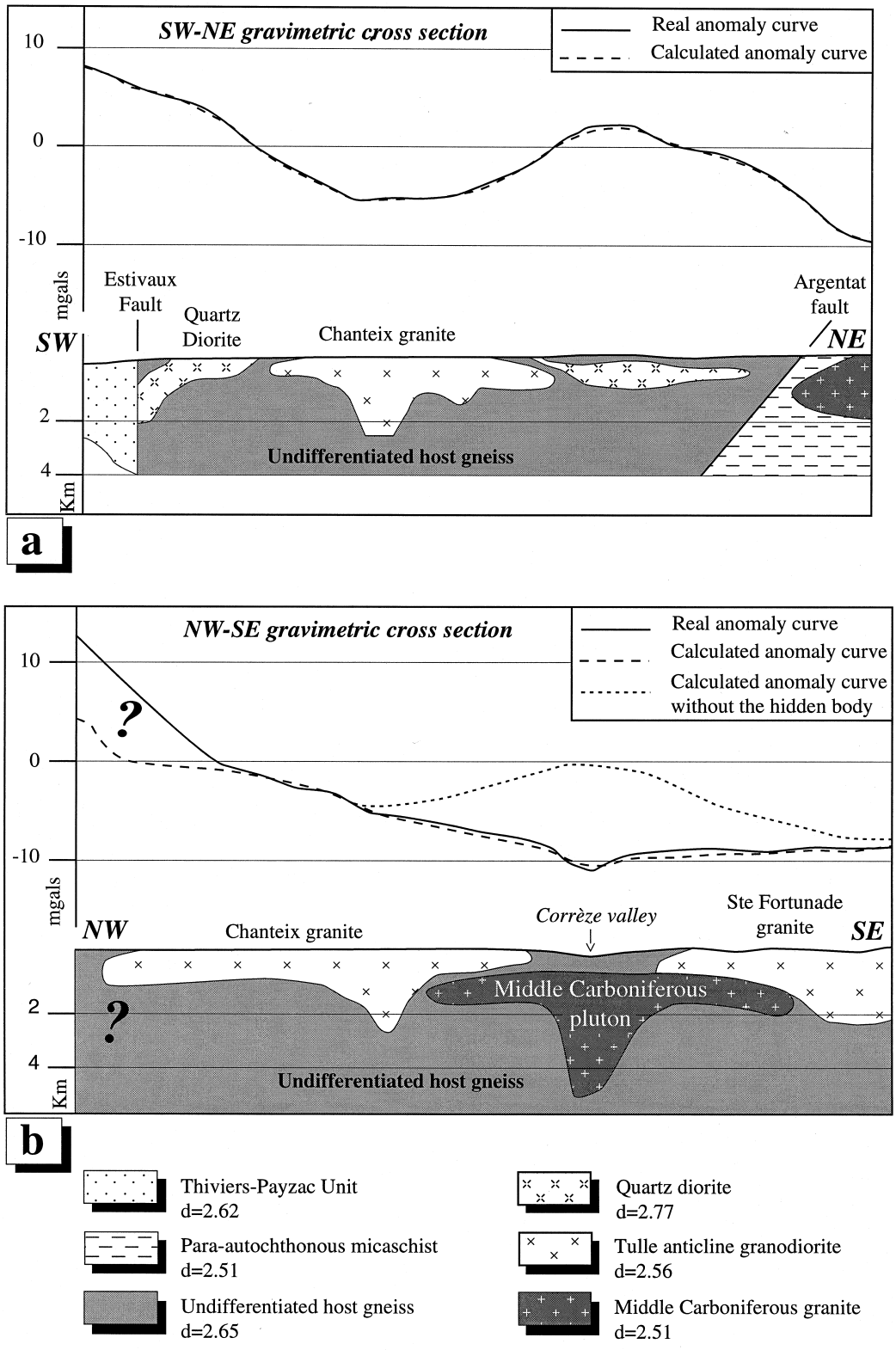

Fig. 11. Modelled 2.5-dimensional gravimetric cross-sections around the Chanteix pluton, located in Fig. 10. (a) SW–NE transverse cross-section. (b) NW–SE longitudinal cross-section.

for a middle Carboniferous age for this hidden body (Bernard-Griffiths, 1975).

Gravimetric modelling suggests that the Chanteix Massif has an average thickness of 1 km and presents a deeper zone of 2.5 km located in the southeastern part of the massif, which is interpreted as the pluton root zone. This asymmetric southeast location of the root zone supports that the pluton was dominantly stretched northwestward in agreement to the regional deformation. The Chanteix body is 15 km long, 10 km

wide and less than 2 km thick, and therefore appears to be a laccolith. By analogy with the Chanteix body, we assume that the Sainte-Fortunade and Albussac massifs have a similar laccolithic shape. The bulk shape and small size of these bodies, which argue for a small volume of intruded magma, do not favour a hot Stokes type of diapiric emplacement. Magma channelling through small conduits such as dykes and sills is more likely (Clemens and Mawer, 1992; Rubin, 1993; Petford *et al.*, 1994).

DISCUSSION AND CONCLUSIONS

Microstructural, TEM and strain analyses allow us to characterize the granite deformation history during its emplacement and cooling. The first event corresponds to a pre-full crystallization deformation responsible for the brittle deformation of early crystallized minerals, like plagioclase, during crystallization of the last fraction of magma (Hibbard, 1986). The second stage which is recognized by quartz texture and TEM analyses corresponds to a high-temperature (near 650°C) solid-state deformation stage which induces quartz prism ⟨*c*⟩ slip responsible for SGBs and the preserved mosaic-like texture of quartz. The last stage is a moderate-temperature (350°C) deformation characterized by basal ⟨*a*⟩ glide and responsible for the ⟨*c*⟩-axis preferred orientation measured with the universal stage. TEM analysis points out that the old high-temperature microstructure is not completely obliterated by the younger low-temperature one.

The shape of the Tulle anticline granites differs from the inverted tear-drop shape experimentally obtained for diapiric models (e.g. Ramberg, 1981; Cruden, 1990; Talbot, 1993). Rim synclines that are predicted to form at the margin of diapirs are also lacking. In addition, the weak ductile deformation at the pluton margins and the discordant contact at the northwestern end of the Chanteix pluton does not support a ballooning emplacement. Structural analysis and gravimetric modelling reveal a laccolithic shape of these bodies which might emplace in a supracrustal level (e.g. Pollard and Johnson, 1973; Corry, 1988). The thin tabular shape of the plutons, the small volume implied and the lack of evidence for vertical displacement of the host rocks also preclude a diapiric emplacement mechanism. In any case, in the upper crust, rheological and thermal contrasts between granite and host rock are high, thus a diapiric process is unlikely for granite emplacement. Moreover, channelling through small conduits such as dykes and sills (Petford *et al.*, 1994) is supported by our field observations of dykes in the host rocks. The mechanisms responsible for emplacement of the main bodies have to be considered with respect to the space problem. As shown above, the fabric patterns of the plutons indicate maximum (X) and intermediate (Y) strain axes parallel and perpendicular to the fold axis, respectively, and constrictional strain that is consistent with granite emplacement related to folding. Owing to very different strain rates, of more than one order of magnitude, magma injection is a nearly instantaneous process compared to folding. Therefore, dyke opening cannot be considered as strictly due to folding but rather enhanced by deformation-related low-stress areas.

Within an anticline, three places are suitable for local formation of low-stress domains, namely: (i) at the exterior part (extrado) of the fold hinge; (ii) perpendicular or at high angles to the hinge; and (iii) along décollement layers in the hinges and limbs. In the Tulle antiform, the first location is not realistic, but the numerous N50E-trending 'hot slickensides' support the presence of décollement layers (Fig. 2). The anisotropy formed by the foliation surface was reused as localized movement zones. Most of the dykes trend NE–SW, but NW–SE-trending dykes are also observed (Fig. 6). These NW–SE-trending dykes indicate that brittle stretching also occurred along the anticline hinge. The 2–2.5 kbar and 220–300°C emplacement conditions, which are those of the brittle–ductile transition zone, are in agreement with an upper crustal setting for emplacement of the Tulle anticline granites.

The following scenario can be proposed (Fig. 12). (1) In the early Carboniferous, at the end of the regional NW–SE thrust tectonics, the intermediate strain axis is a shortening direction ($Y < 0$). This NE–SW shortening is responsible for an arched shape of the proto-Tulle antiform. Owing to the rheological behaviour near the brittle–ductile transition zone, buckling leads to low-stress domains allowing slip on the preexisting foliation and crack opening at high angles to the fold axis. (2) Such low-stress domains are favourable places for magma injection (Fig. 12). The emplacement and fabrics of the granites are the result of the interaction between: (i) a tectonic process, namely a regional disharmonic folding which allows magma to flow in the weakened parts of the fold; and (ii) a magmatic process, namely forceful injections which might be responsible for buckling of the foliation. The role of magma overpressure often advocated to account for overthickening and deformation of the overburden (e.g. Pollard and Johnson, 1973; Corry, 1988) is not demonstrated in our case. However, the mean volume of the Chanteix body is estimated around 600 km^3 and the total volume of the outcropping plutons is about 1500 km^3. Such an amount of magma can mechanically account for an uplift of several hundred metres of the pluton roof. (3) In the last stage of magma crystallization, a vertical shortening is responsible for the folding and flat foliation development in the dykes. As mentioned above, the same NW–SE maximum stretching direction for the 360 Ma flat-lying structures, upright folding and granite emplacement suggests that

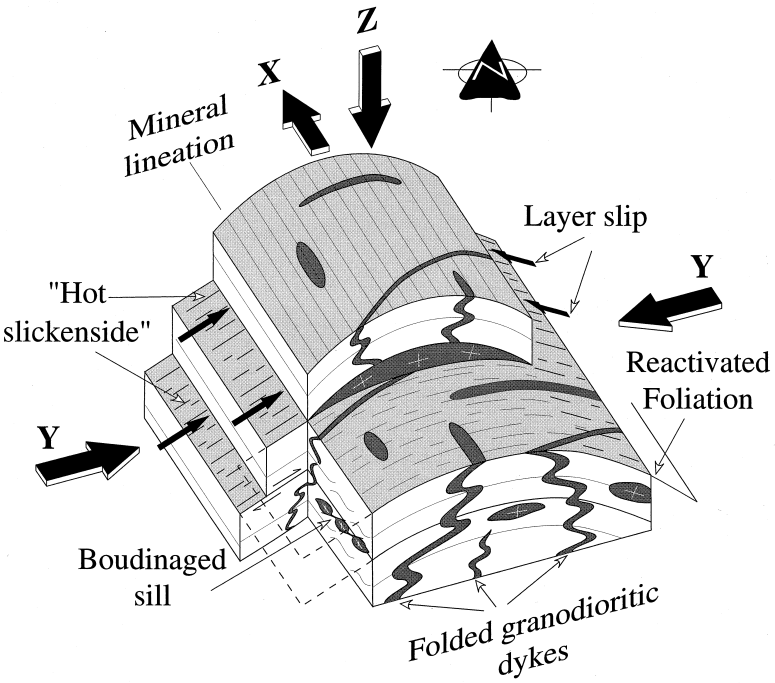

Fig. 12. Emplacement model for the Tulle anticline granite and related dykes. Magma fills voids opened by layer slip in the hinge zone of a buckle fold ($X > Y > Z$: principal axes of the strain ellipsoid).

these two events belong to a deformation continuum. The lack of axial-planar cleavage both in the upright folds and in the dykes shows that shortening along the NE–SW-trending *Y*-axis was rather weak. Lastly, the fold arcuation was probably accentuated during the middle Carboniferous extensional tectonics in relation with emplacement of leucogranite plutons in antiformal structures, as recognized elsewhere in the French Massif Central (Faure, 1995).

Acknowledgements—J. C. Doukhan helped us to operate TEM and to improve the discussion on quartz microstructure. P. Ledru (BRGM/DR/MGG) is thanked for fruitful discussion and allowing the use of unpublished radiometric dates. Gravimetric modelling was made as part of the GéoFrance 3D program. C. Mennechet (BRGM/SGN/I2G) provided facilities to compute gravimetric cross-sections. S. Paterson is thanked for constructive advice to improve a first draft of the manuscript. We also thank K. Benn and A. Vauchez for their helpful reviews and constructive criticisms. This article is the GéoFrance 3D contribution number 23.

REFERENCES

Alinat, M. (1975) *Le zircon dans les roches de la série métamorphique de "l'Anticlinal" de Tulle (Corrèze, Massif Central français), applications pétrogénétiques*. Thèse 3ème cycle, Université de Nice.

Ardell, A. J., Christie, J. M. and McCormick, J. W. (1974) Dislocation images in quartz and the determination of Burgers vector. *Philosophical Magazine* **29,** 1399–1411.

Bernard-Griffiths, J. (1975) *Essai sur la signification des âges au strontium dans une série métamorphique: le Bas Limousin (Massif Central français)*. Thèse 3ème cycle, Université de Clermont Ferrand, Annales Scientifiques de l'Université de Clermont Ferrand, **55**.

Bernard-Griffiths, J. and Vachette, M. (1970) Age cambrien des migmatites de l'anticlinal de Tulle (Massif Central français) et ses relations avec l'âge du granite dit tardimigmatitique de Cornil. *Comptes rendus de l'Académie des Sciences* **270,** 916–919.

Blumenfeld, P., Mainprice, D. and Bouchez, J. L. (1985) Glissement de direction ⟨*c*⟩ dominant dans le quartz de filons de granite cisaillés en conditions sub-solidus (Vosges, France). *Comptes rendus de l'Académie des Sciences* **301,** 1303–1308.

Bouchez, J. L., Delas, C., Gleizes, G. and Nedelec, A. (1992) Submagmatic microfractures in granites. *Geology* **20,** 35–38.

Bouchez, J. L., Tubia, J. M. and Mainprice, D. (1985) Déformation naturelle du quartz: coexistence des systèmes de glissement de direction ⟨*a*⟩ et ⟨*c*⟩ à haute température (migmatites de la nappe d'Ojén, Espagne). *Comptes rendus de l'Académie des Sciences* **301,** 841–846.

Castro, A. (1987) On granitoid emplacement and related structures. A review. *Geologische Rundschau* **76,** 101–124.

Clemens, J. D. and Mawer, C. K. (1992) Granitic magma transport by fracture propagation. *Tectonophysics* **184,** 339–360.

Corry, C. E. (1988) *Laccoliths: Mechanics of Emplacement and Growth*. Geological Society Special Paper, **220**.

Cruden, A. (1990) Flow and fabric development during the diapiric rise of magma. *Journal of Geology* **98,** 681–698.

Dunnet, D. (1969) A technical method of finite strain analysis using elliptical particles. *Tectonophysics* **7,** 117–136.

Duthou, J. L. (1977) *Chronologie Rb–Sr et géochimie des granitoïdes d'un segment de la chaîne varisque. Relations avec le métamorphisme: le Nord-Limousin*. Thèse 3ème cycle, Université de Clermont Ferrand, Annales Scientifiques de l'Université de Clermont Ferrand, **63**.

Etchecopar, A. (1977) Kinematic model of progressive deformation in polycrystalline aggregates. *Tectonophysics* **39,** 121–139.

Etchecopar, A. and Vasseur, G. (1987) A 3-D kinematic model of fabric development in polycrystalline aggregates: comparison with experimental and natural examples. *Journal of Structural Geology* **9,** 705–717.

Faure, M. (1995) Late Carboniferous extension in the Variscan French Massif Central. *Tectonics* **14,** 132–153.

Faure, M., Sun, Y., Shu, L. and Charvet, J. (1996) Extensional tectonics within a subduction-type orogen, The case study of the Wugongshan dome (Jiangxi Province, Southeastern China). *Tectonophysics* **263,** 77–106.

Floc'h, J. P. (1983) *La série métamorphique du Limousin central*. Thèse d'Etat. Université de Limoges.

Gapais, D. (1987) *Les orthogneiss: structures, mécanismes de déformation et analyse cinématique*. Thèse d'Etat. Université de Rennes.

Gapais, D. and Barbarin, B. (1986) Quartz fabric transition in a cooling syntectonic granite (Hermitage massif, France). *Tectonophysics* **125,** 357–370.

Guillot, P. L. (1981) *La série métamorphique du Bas Limousin: de la vallée de l'Isle à la vallée de la Vézère, le socle en bordure du Bassin aquitain*. Thèse d'Etat. Université d'Orléans.

Guillot, P. L. and Feix, I. (1985) *La dislocation d'Argentat, une frontière majeur dans le Massif Central Occidental*. Progamme GPF1, Thème, **3,** 71–85.

Hibbard, M. J. (1979) Myrmekites as a marker between preaqueous and postaqueous phase saturation in granitic systems. *Geological Society American Bulletin* **90,** 1047–1062.

Hibbard, M. J. (1986) Deformation of incompletely crystallized systems: granitic gneisses and their tectonic implications. *Journal of Geology* **95,** 543–561.

Hibbard, M. J. and Watters, R. J. (1985) Fracturing and diking in incompletely crystallized granitic plutons. *Lithos* **18,** 1–12.

Hill, E. J., Baldwin, S. L. and Lister, G. S. (1992) Unroofing of active metamorphic core complexes in the d'Entrecasteaux region, Papua New Guinea. *Geology* **20,** 907–910.

Hirsh, P. B., Howie, A., Nicholson, R. B., Pashley, D. W. and Whelan, M. J. (1965) *Electron Microscopy of Thin Crystals*. Butterworths, London.

Holm, D. K., Snow, J. K. and Lux, D. R. (1992) Thermal and barometric constraints on the intrusive and unroofing history of the Black Mountains: implications for timing, dip, and kinematics of detachment faulting in the Death Valley region, California. *Tectonics* **11,** 507–522.

Hutton, D. H. W. (1988) Granite emplacement mechanisms and tectonic controls: inferences from deformation studies. *Transactions of the Royal Society of Edinburgh, Earth Science*, **79,** 245–255.

Hutton, D. H. W. and Reavy, R. J. (1992) Strike-slip tectonics and granite petrogenesis. *Tectonics* **11,** 960–967.

Jessell, M. W. and Lister, G. S. (1990) A simulation of temperature dependence of quartz fabrics. In *Deformation Mechanisms, Rheology and Tectonics*, eds R. J. Knipe and E. H. Rutter, pp. 353–362. Geological Society, London, Special Publication, **54**.

Lafon, J. M. (1986) *Géochronologie U–Pb appliquée à deux segments du Massif Central français: Le Rouergue oriental et le Limousin central*. Thèse de l'Université de Montpellier.

Lagarde, J. L., Dallain, C., Ledru, P. and Courrioux, G. (1994) Strain patterns within the late Variscan granitic dome of Velay, french Massif Central. *Journal of Structural Geology* **16,** 839–852.

Law, R. D. (1987) Heterogeneous deformation and quartz crystallographic fabric transitions: natural examples from the Moine Thrust zone at the Stack of Glencoul, northern Assynt. *Journal of Structural Geology* **9,** 819–833.

Law, R. D. (1990) Crystallographic fabric: a selective review of their applications to research in structural geology. In *Deformation Mechanisms, Rheology and Tectonics*, eds R. J. Knipe and E. H. Rutter, pp. 335–352. Geological Society, London, Special Publication, **54**.

Ledru, P. and Autran, A. (1987) L'édification de la chaîne varisque dans le Limousin. Rôle de la faille d'Argentat à la limite Limousin–Millevaches. Programme G.P.F, Document B.R.G.M. **140,** pp. 87–106.

Ledru, P., Lardeau, J. M., Santallier, D., Autran, A., Quenardel, J. M., Floc'h, J. P., Lerouge, G., Maillet, N., Marchand, J. and Ploquin, A. (1989) Où sont les nappes dans le Massif Central français? *Bulletin de la Société Géologique de France* **V,** 605–618.

Lister, G. S. and Dornsiepen, U. F. (1982) Fabric transition in the Saxony granulite terrain. *Journal of Structural Geology* **4,** 81–92.

Lister, G. S. and Hobbs, B. E. (1980) The simulation of fabric development during plastic deformation and its application to quartzite: the influence of deformation history. *Journal of Structural Geology* **2,** 355–370.

Mainprice, D., Bouchez, J. L., Blumenfeld, P. and Tubia, J. M. (1986) Dominant *c* slip in naturally deformed quartz. Implications for dramatic plastic softening at high temperature. *Geology* **14,** 819–822.

Marre, J. (1982) Méthode d'Analyse Structurale des Granitoïdes. In *Manuel et méthodes*. BRGM, Orléans.

Mattauer, M., Brunel, M. and Matte, P. (1988) Failles normales ductiles et grands chevauchements. Une nouvelle analogie entre l'Himalaya et la chaîne hercynienne du Massif Central français. *Comptes rendus de l'Académie des Sciences* **306,** 671–676.

Matte, P. (1986) Tectonics and plate tectonics model for the Variscan of Europe. *Tectonophysics* **126,** 329–374.

Naney, M. T. (1983) Phase equilibria of rock-forming ferromagnesian silicates in granitic systems. *American Journal of Science* **283,** 993–1033.

Panozzo, R. (1987) Two-dimensional strain determination by the inverse SURFOR wheel. *Journal of Structural Geology* **9,** 115–187.

Paterson, S. R. and Tobisch, O. T. (1988) Using pluton ages to date regional deformation: problems with commonly used criteria. *Geology* **16,** 1108–1111.

Paterson, S. R., Vernon, R. H. and Tobisch, O. T. (1989) A review of criteria for the identification of magmatic and tectonic foliations in granitoids. *Journal of Structural Geology* **11,** 349–363.

Petford, N., Lister, J. R. and Kerr, R. C. (1994) The ascent of felsic magma in dykes. *Lithos* **32,** 161–168.

Pin, C. and Peucat, J. J. (1986) Age des épisodes de métamorphisme paléozoïque dans le Massif Central et le Massif Armoricain. *Bulletin de la Société Géologique de France* (8II3), 461–469.

Plouff, D. (1975) *Derivation of formulas and Fortran programs to compute gravity anomalies of prisms*. United States Geological Survey, Open-file Report, Vol. 83, pp. 1–53.

Pollard, D. D. and Johnson, A. M. (1973) Mechanics of growth of some laccolithic intrusions in the Henry Mountains, Utah, Part II; Bending and failure of overburden and sill formation. *Tectonophysics* **18,** 311–354.

Ramberg, H. (1981) *Gravity, Deformation and the Earth's Crust in Theory, Experiments and Geological Applications*. Academic Press, London.

Ramsay, J. G. (1967) *Folding and Fracturing of Rocks*. McGraw-Hill, New York.

Roig, J. Y. (1997) *Evolution tectono-métamorphique d'un segment de la chaîne hercynienne. Rôle du plutonisme dans la caractérisation des tectoniques du Sud-Limousin (Massif Central français)*. Thèse de l'Université d'Orléans.

Roig, J. Y. and Faure, M. (1995) La déformation du quartz dans un pluton syntectonique mis en place pendant l'extension Carbonifère supérieur du Massif Central français (le leucogranite de Chambles, Massif du Velay). *Comptes rendus de l'Académie des Sciences* **321,** 789–796.

Roig, J. Y. and Faure, M. (1996) Plutonisme et plissement: l'exemple de l'anticlinal de Tulle. In *16ème Réunion des Sciences de la Terre (Abstract Volume)*. Société Géologique de France, Paris.

Roig, J. Y., Faure, M. and Ledru, P. (1996) Polyphase wrench tectonics in the southern French Massif Central: kinematic inferences from pre- and syntectonic granitoids. *Geologische Rundschau* **85,** 138–153.

Rubin, A. M. (1993) Dikes vs diapirs in viscoelastic rock. *Earth and Planetary Science Letters*, **119,** 641–659.

Santallier, D. (1981) *Les roches métamorphiques du Bas-Limousin, Massif Central (France)*. Thèse d'Etat, Université Orléans.

Simpson, C. and Wintsch, R. P. (1989) Evidence for deformation induced K-feldspar replacement by myrmekite. *Journal of Metamorphic Geology* **4,** 261–275.

Soula, J. C. (1982) Characteristics and mode of emplacement of gneiss domes and plutonic domes in central–eastern Pyrénées. *Journal of Structural Geology* **4,** 313–342.

Talbot, C. J. (1993) Spreading of salt structures in the Gulf of Mexico. *Tectonophysics* **228,** 151–166.

Tommasi, A., Vauchez, A., Fernandes, L. A. D. and Porcher, C. C. (1994) Magma-assisted strain localization in an orogen-parallel transcurrent shear zone of southern Brazil. *Tectonics* **13,** 421–437.

Trépied, L., Doukhan, J. C. and Paquet, J. (1980) Sub-grain boundaries in quartz. Theoretical analysis and microscopic observation. *Physics and Chemistry of Minerals* **5,** 201–218.

Vernon, R. H. (1991) Questions about myrmekite in deformed rocks. *Journal of Structural Geology* **13,** 979–985.